REGULAR ARTICLE

blood advances

Exogenous mitochondrial transfer and endogenous mitochondrial fission facilitate AML resistance to OxPhos inhibition

Kaori Saito,[1] Qi Zhang,[2] Haeun Yang,[1] Kotoko Yamatani,[1,3] Tomohiko Ai,[1] Vivian Ruvolo,[4] Natalia Baran,[2] Tianyu Cai,[2] Helen Ma,[2] Rodrigo Jacamo,[4] Vinitha Kuruvilla,[2] Junichi Imoto,[5] Sonoko Kinjo,[5] Kazuho Ikeo,[5] Kaori Moriya,[6] Koya Suzuki,[1,7] Takashi Miida,[1] Yong-Mi Kim,[8] Christopher P. Vellano,[9] Michael Andreeff,[4] Joseph R. Marszalek,[9] Yoko Tabe,[1,4,10] and Marina Konopleva[2]

[1]Department of Clinical Laboratory Medicine, Juntendo University Graduate School of Medicine, Tokyo, Japan; [2]Section of Leukemia Biology Research, Department of Leukemia, The University of Texas MD Anderson Cancer Center, Houston, TX; [3]Research Fellow of the Japan Society for the Promotion of Science, Tokyo, Japan; [4]Section of Molecular Hematology and Therapy, Department of Leukemia, The University of Texas MD Anderson Cancer Center, Houston, TX; [5]Center for Information Biology, National Institute of Genetics, Shizuoka, Japan; [6]Laboratory of Morphology and Image Analysis, and [7]Research Institute for Diseases of Old Age, Juntendo University Graduate School of Medicine, Tokyo, Japan; [8]Pediatrics and Pathology, Keck School of Medicine, University of Southern California, Los Angeles, CA; [9]TRACTION, Therapeutics Discovery Division, The University of Texas MD Anderson Cancer Center, Houston, TX; and [10]Department of Next Generation Hematology Laboratory Medicine, Juntendo University Graduate School of Medicine, Tokyo, Japan

Key Points

- OxPhos inhibition induces mitochondrial trafficking from BM stroma cells to AML cells accompanied by mitochondrial fission and mitophagy.
- Mitochondrial coupling and crosstalk with BM stroma cells facilitate the development of AML cell resistance to OxPhos inhibition.

Acute myeloid leukemia (AML) cells are highly dependent on oxidative phosphorylation (OxPhos) for survival, and they continually adapt to fluctuations in nutrient and oxygen availability in the bone marrow (BM) microenvironment. We investigated how the BM microenvironment affects the response to OxPhos inhibition in AML by using a novel complex I OxPhos inhibitor, IACS-010759. Cellular adhesion, growth, and apoptosis assays, along with measurements of expression of mitochondrial DNA and generation of mitochondrial reactive oxygen species indicated that direct interactions with BM stromal cells triggered compensatory activation of mitochondrial respiration and resistance to OxPhos inhibition in AML cells. Mechanistically, inhibition of OxPhos induced transfer of mitochondria derived from mesenchymal stem cells (MSCs) to AML cells via tunneling nanotubes under direct-contact coculture conditions. Inhibition of OxPhos also induced mitochondrial fission and increased functional mitochondria and mitophagy in AML cells. Mitochondrial fission is known to enhance cell migration, so we used electron microscopy to observe mitochondrial transport to the leading edge of protrusions of AML cells migrating toward MSCs. We further demonstrated that cytarabine, a commonly used antileukemia agent, increased mitochondrial transfer of MSCs to AML cells triggered by OxPhos inhibition. Our findings indicate an important role of exogenous mitochondrial trafficking from BM stromal cells to AML cells as well as endogenous mitochondrial fission and mitophagy in the compensatory adaptation of leukemia cells to energetic stress in the BM microenvironment.

Introduction

The interaction between stromal cells in the bone marrow (BM) microenvironment with acute myeloid leukemia (AML) cells promotes the survival of AML cells.[1-3] AML cells are also highly dependent on oxidative phosphorylation (OxPhos) and continually adapt to fluctuations in nutrient and oxygen availability in the BM microenvironment.[4-7] In a previous study, we reported anti-AML activity of the first-in-class OxPhos inhibitor IACS-010759, whose mechanisms of action include

Submitted 22 October 2020; accepted 9 June 2021; prepublished online on *Blood Advances* First Edition 10 September 2021; final version published 25 October 2021. DOI 10.1182/bloodadvances.2020003661.

The full-text version of this article contains a data supplement.

deprivation of energy, depletion of aspartate, and increase in intracellular reactive oxygen species (ROS).[8] Recent studies demonstrated that ROS trigger BM stromal cells to transfer their mitochondria to leukemia cells through tunneling nanotubes (TNTs) under conditions of stress or chemotherapy.[9-11] Transfer of functional mitochondria has been shown to increase mitochondrial respiration and the production of adenosine triphosphate in recipient cells, leading to improved functional activity.[12]

In preclinical studies, the majority of AML tumor models were responsive to OxPhos inhibition through targeting of complex I,[8] but it is unknown how the BM microenvironment affects these responses. Despite promising preclinical studies, carboxyamidotriazole, a putative complex I inhibitor, failed to demonstrate clinical benefit in multiple solid tumors.[13] The phase I trial of BAY87-2243 (a novel complex I inhibitor that demonstrated antitumor efficacy without toxicity in mice) was terminated because of unexpected toxicities in humans.[14] These findings indicate the narrow therapeutic window of OxPhos inhibitors that have limited potency in humans and support the need for relevant preclinical models geared toward understanding mitochondrial biogenesis and the crosstalk between tumor cells and their microenvironment.

In this study, we investigated the mechanisms by which the BM microenvironment facilitates development of secondary resistance to OxPhos inhibition in AML cells. We observed that treatment with an OxPhos inhibitor (OxPhosi) induced adhesion of AML cells to BM mesenchymal stem cells (MSCs), formation of TNTs, mitochondrial transfer from MSCs to AML cells, and mitochondrial fission. The mitochondria transferred from MSCs were then degraded by mitophagy in AML cells. Our findings indicate that under conditions of OxPhos inhibition, AML cells successfully replenish functional mitochondria through exogenous transfer of mitochondria supplied by MCSs and endogenous fission of healthy mitochondria. These processes together facilitate the development of resistance to OxPhos inhibition in AML cells by maintaining their mitochondrial function.

Methods

Primary samples, cell lines, culture conditions, and reagents

Primary AML cells were obtained from 26 AML patients, and primary MSCs were obtained from healthy donor BM. OxPhosi-sensitive OCI-AML3 cells,[8] OxPhosi-resistant MOLM13 cells,[8] U937 cells,[8] and MSCs were transduced with lentiviral vectors encoding a fusion of the sequence of a mitochondrial matrix enzyme (pyruvate dehydrogenase E1 alpha 1 [*PDHA1*]) to the amino terminus of the green fluorescent protein copGFP (AML cells) or of the red fluorescent protein dsRed (MSCs). The OxPhosi IACS-010759[8] was obtained from the Institute for Applied Cancer Science at MD Anderson Cancer Center (Houston, TX). Cytarabine, cytochalasin D, the intercellular adhesion molecule 1 (ICAM-1) neutralizing antibody, natalizumab, dansylcadaverine, and bafilomycin were used as described.

Types of cell analyses

Cell viability and proliferation were assessed by cell counters using the Trypan blue exclusion method or MTS assays. Apoptotic cell death was analyzed by annexin V/propidium iodide staining and flow cytometry as described elsewhere.[15] Total cellular ROS production was quantified by using a CellROX Deep Red Flow Cytometry Assay Kit. The cap analysis gene expression (CAGE) protocol was described previously.[16] Normalized data were subjected to EdgeR and DEGseq (an R package for identifying differentially expressed genes from RNA sequencing data)[17,18]; gene set enrichment analysis[19] was performed to determine differences in expression in gene promoters. Adhesion of AML cells to MSCs was assessed by adhesion assays described elsewhere.[20]

The Seahorse XF24 Extracellular Flux analyzer (Seahorse Bioscience) was used to measure the oxygen consumption rate (OCR) of OCI-AML3 and MOLM13 cells and MSCs according to the manufacturer's instructions.[21] Briefly, AML cells were cultured with or without the indicated concentrations of IACS-010759 and/or an anti-ICAM-1 antibody in the presence or absence of MSCs for 2 hours. Before use in the extracellular flux assays, cocultured AML cells were separated from the MSC monolayer by careful pipetting. AML cells were counted, and 5×10^5 cells were added to each well for the extracellular flux assays. For MSCs, 6×10^4 cells were added to each well with or without treatment by IACS-010759 (30 nM) for 2 hours. Three technical replicates for each condition were plated.

Immunoblot analysis was performed as previously described.[15] OCI-AML3 and MOLM13 cells stably transfected with *PDHA1*-GFP and/or MSCs transfected with *PDHA1*-dsRed were plated . Confocal fluorescence images were captured with a confocal microscope. We used a Mitophagy Detection Kit (Dojindo Molecular Technologies) to detect mitophagy.[22] Mitochondrial membrane potentials were measured by using a JC-1 Mitochondrial Membrane Potential Assay Kit. For electron microscopy analysis, cells were fixed with 2% glutaraldehyde, and for immunoelectron microscopy analysis, cells were fixed with 2% paraformaldehyde and 0.025% glutaraldehyde and were examined by using a Hitachi HT7700 transmission electron microscope. A Human Mitochondrial DNA Monitoring Primer Set (Takara Bio) was used for quantitative polymerase chain reaction.

In vivo mouse experiments for CAGE analysis

NOD-*scid* IL2Rγ^{null} (NSG) mice 6 to 8 weeks old were injected with 1 million AML patient-derived xenograft (PDX) cells. Four weeks after confirmation of engraftment in peripheral blood by hCD45$^+$ flow cytometry, the mice were randomly assigned to receive IACS-010759 (5.0 mg/kg; 5 days on and 2 days off) or vehicle (solvent-only control) by oral gavage ($n = 3$ in each group). Mice were euthanized when full engraftment was detected by flow cytometry or when any sign of morbidity was observed. Spleen cells were collected and enriched for human cells by depletion of mouse cells with an EasySep Mouse/Human Chimera Isolation Kit.

Murine/human mtDNA quantification in the in vivo mouse model

Human primary AML cells were injected into NSG mice. The ratio of murine to human mitochondrial DNA (mtDNA) in spleen-resident AML cells was determined after oral treatment once per day with IACS-010759 (5.0 mg/kg per day; 5 days on and 2 days off for 21 days) or vehicle using the Mouse Feeder Cell Quantification Kit.

Statistical analyses

GraphPad Prism 9 was used for statistical analysis. All values are expressed as the mean ± standard deviation (SD). Differences between groups were assessed by 2-way analysis of variance or

Student *t* test. $P < .05$ was considered statistically significant. Additional details regarding methods are provided in the supplemental Materials and Methods.

Results

OxPhos inhibition activates cell adhesion in AML cells

We first investigated the role of BM stromal cells, the obligate component of the BM microenvironment, in the resistance of AML cells to OxPhos inhibition. Because availability of primary AML cells was limited, we used OxPhosi-sensitive and OxPhos-dependent OCI-AML3 cells and OxPhosi-resistant MOLM13 and U937 cells.[8] As shown in Figure 1A, MSC coculture reduced the inhibitory effects of IACS-010759 on cell growth in sensitive OCI-AML3 cells but not in resistant MOLM13 cells. IACS-010759-induced inhibition of cell growth was also significantly reduced by coculturing less sensitive U937 cells with MSCs. No significant inhibition of cell growth by IACS-010759 was observed in MSCs.

To investigate the molecular mechanisms of resistance to OxPhos inhibition, we performed CAGE transcriptome analyses[23] on OCI-AML3 cells that were cultured with or without BM-derived MSCs in the absence or presence of 30 nM IACS-010759 for 15 hours. In OCI-AML3 cells cocultured with MSCs (supplemental Figure 1), inhibition of OxPhos upregulated the gene signatures of adhesion-related extracellular organization and tube morphogenesis (supplemental Table 1). In contrast, inhibition of OxPhos activated the endoplasmic reticulum stress response and intrinsic apoptotic signaling pathways without affecting adhesion-related pathways in OCI-AML3 cells cultured alone. To evaluate whether inhibition of OxPhos enhances the adhesion of AML cells to MSCs, we analyzed the adhesion of OCI-AML3 cells to MSCs using a coculture system. A concentration of 30 nM IACS-010759 significantly stimulated the adherence of OCI-AML3 cells to MSCs (Figure 1B).

We then performed CAGE analysis using peripheral blood samples from 26 patients with primary AML. Table 1 shows the clinical information for the patients from whom samples were obtained, including driver genetic mutations. The sensitivity of primary AML cells from each patient was detected by treatment with 100 nM IACS-010759 for 72 hours. The samples were then classified as sensitive ($n = 16$) or resistant ($n = 10$) depending on the fold increase in the percentage of annexin V^+ cells, with an arbitrary cutoff value of 3.0 (supplemental Figure 2). To assess differences in baseline promoter gene expression between sensitive and resistant cells, we conducted CAGE analysis on untreated primary AML cells. Analysis using the Bioconductor EdgeR package ($\log_2$ fold change, >2.0; false discovery rate [FDR], <0.05) detected 16 gene promoters with higher baseline expression in OxPhosi-resistant AML samples than in sensitive samples. Most of these genes were related to cell adhesion, migration, and the rho GTPase family of genes, which modulates intracellular actin dynamics (Table 2). We observed a modest increase in expression of the promoters of the cell adhesion–related gene *C2CD4B*[24] and of the rho GTPase family genes *RET*,[25] *RCBTB2*,[26] and *RASL11A*[27] in OxPhosi-resistant AML samples compared with sensitive ones ($\log_2$ fold change, >2.0; FDR, <0.01 [EdgeR]) (supplemental Figure 3).

Next, we investigated changes in cellular energy metabolism under OxPhos inhibition by using an extracellular flux assay of OCI-AML3, MOLM13, and U937 cells with and without MSC coculture. In cocultured AML cells, the OCR was measured after AML cells were separated from the MSC monolayer by carefully pipetting. The baseline OCR of OxPhosi-resistant MOLM13 cells was higher than that of OxPhosi-sensitive OCI-AML3 cells, and MSC coculture decreased the baseline OCR compared with the single-culture condition in all tested cells (Figure 1C; supplemental Figure 4). As shown in Figure 1C, IACS-010759 decreased the OCR in both cell lines but more potently in OCI-AML3 cells. OCR depletion triggered by IACS-010759 was significantly suppressed in OCI-AML3 cells under MSC coculture conditions but not in MOLM13 cells (percent decrease of OCR [shown hereafter as mean ± SD] in single culture vs MSC coculture: OCI-AML3, 92% ± 2% vs 67% ± 2%; $P = .04$; MOLM13, 71% ± 4% vs 58% ± 6.6%; $P = .24$). In U937 cells with intermediate sensitivity to IACS-010759, MSC coculture reduced the cell growth–inhibitory effects of IACS-010759 by an amount similar to that for OCI-AML3 cells (Figure 1A) and similarly suppressed depletion of OCR triggered by IACS-010759 (percent OCR reduction: U937 alone, 81% ± 2% vs U937 + MSC, 47% ± 5%; $P = .01$, supplemental Figure 4). These results suggest that MSCs support at least partial reversal of the metabolic suppression caused by OxPhos inhibition in AML cells. Considering a 10-fold difference in the numbers of AML cells (5×10^5) and MSCs (6×10^4) for the OCR measurement, the baseline OCR of MSCs was approximately equal to that of AML cells. The OCR inhibitory effect of IACS-010759 in MSCs was modest compared with that in AML cells (percent decrease of OCR, 49% ± 11%; Figure 1D), and no changes were detected in viability or annexin of MSCs (data not shown).

To determine whether the suppression of OxPhosi-induced metabolic blockade by MSCs would translate into rescue of AML cell viability, we investigated IACS-010759-induced apoptotic effects in cocultured AML cells. To examine whether the effect of MSCs is the result of direct cellular contact or of factors secreted by stromal cells, we used annexin V flow cytometry to compare the induction of apoptosis in OCI-AML3 cells cultured in various conditions: with or without an OxPhosi, with or without MSC coculture, and adherence or nonadherence (floating or upper compartment of a transwell insert) to MSCs. As shown in Figure 1E-F, OxPhos inhibition induced apoptotic cell death in AML cells cultured in medium only. In turn, coculture with MSCs rescued OCI-AML3 cells from apoptosis induced by OxPhos inhibition, and cells that adhered to MSCs were more profoundly protected than were nonadherent cells (floating or in the upper transwell insert). Conversely, a statistically significant reduction in the number of annexin$^+$ cells was observed with floating nonadherent cells in upper transwell inserts under MSC coculture conditions compared with cells cultured alone. These findings indicate that soluble factors contribute to protecting AML cells from apoptosis in the presence of BM stromal cells. Thus, BM stromal cells, in particular those in direct contact with leukemia cells and aided by secreted factors, play a key role in the microenvironment-mediated protection of AML cells from metabolic stress caused by OxPhos blockade.

OxPhos inhibition induces mitochondrial transfer from MSCs to AML cells

Previous studies demonstrated that the direct transfer of mitochondria from BM stromal cells may facilitate the production of OxPhos and adenosine triphosphate in leukemia cells.[10,11] We therefore hypothesized that the trafficking of mitochondria from BM stromal cells to AML cells could be a mechanism of acquired resistance to OxPhos

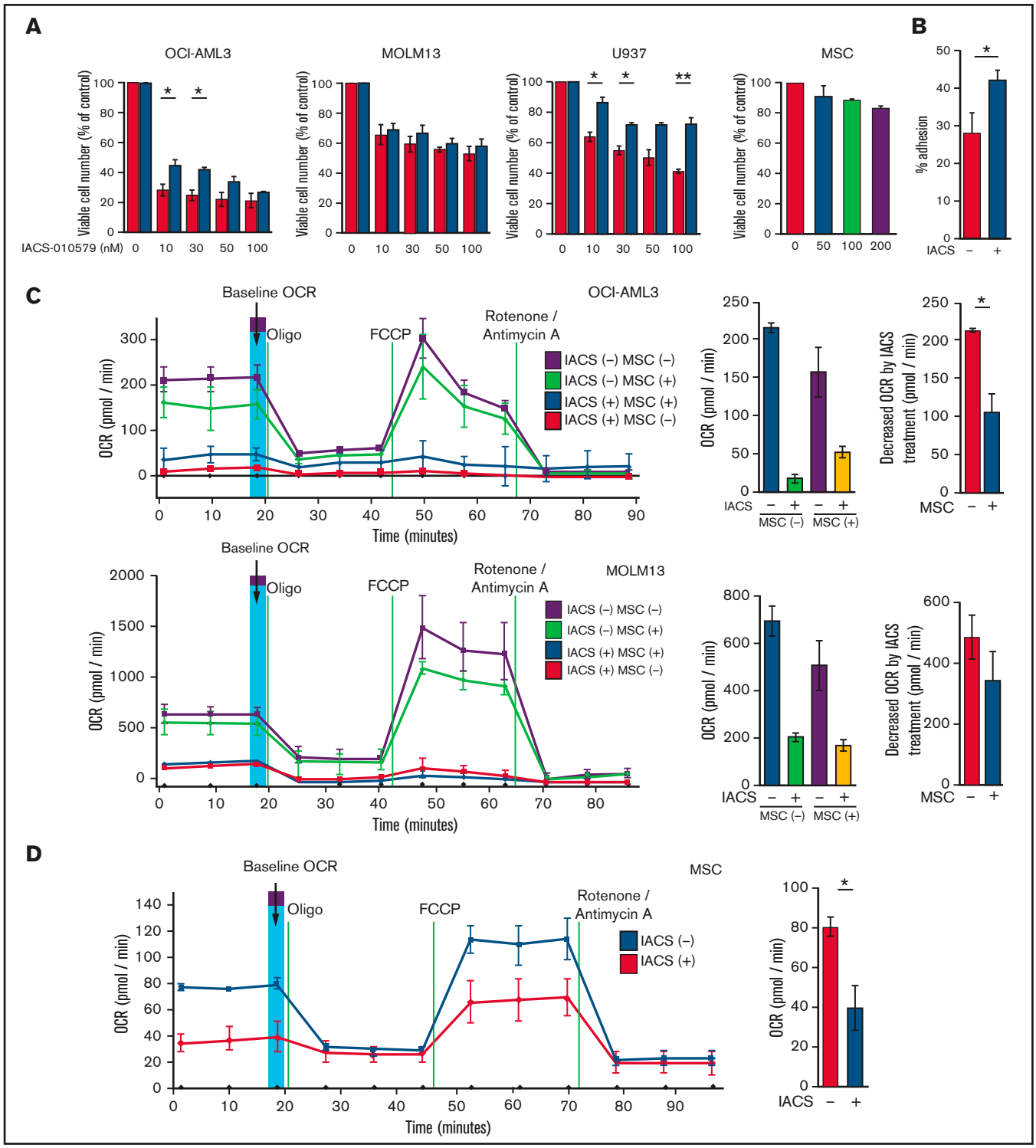

Figure 1.

inhibition. To differentiate mitochondria by their origin, we used OCI-AML3 cells and OxPhosi-resistant MOLM13 cells stably transfected with mitochondria-targeted *PDHA1*-GFP and MSCs transfected with *PDHA1*-dsRed (Figure 2A, left upper panel). A representative confocal image of the dual fluorescence (GFP and dsRed)–positive OCI-AML3 cells cocultured with MSCs in the presence of 30 nM IACS-010759 for 72 hours is shown in Figure 2A (left lower panel). The fluorescence ratios of cells with dual fluorescence were measured in nonadherent OCI-AML3 and MOLM13 cells in the absence and presence of OxPhos inhibition. Interestingly, the percentage of

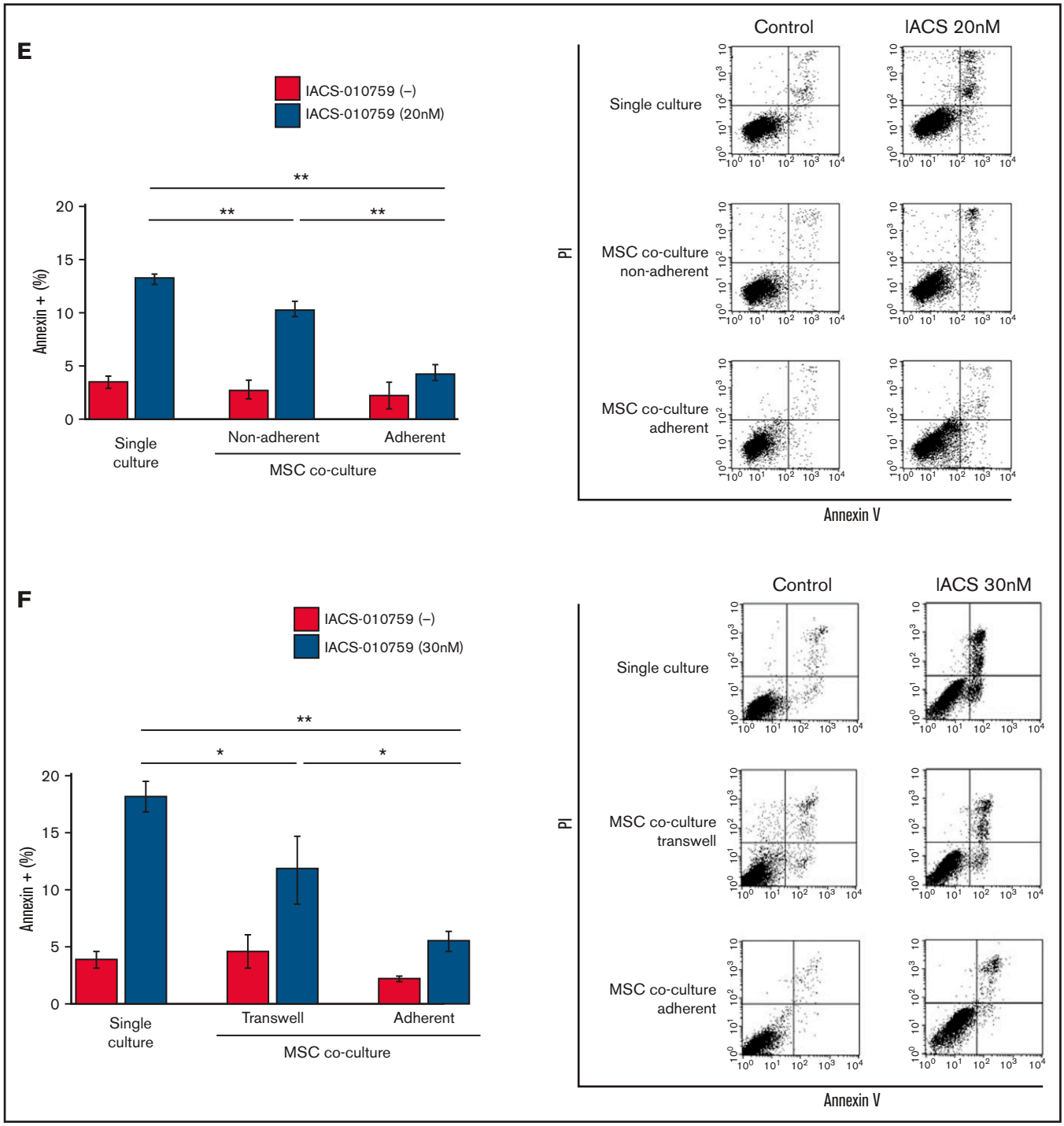

Figure 1. Differentially expressed promoters in OxPhosi-resistant and OxPhosi-sensitive AML cells cocultured with MSCs are associated with reduced antileukemic efficacy of OxPhos inhibition. (A) OCI-AML3, MOLM13, and U937 cells were treated with the indicated doses of the OxPhosi IACS-010759 for 72 hours in the presence or absence of MSCs. The number of viable cells (percent of control) was determined with a Vi-Cell XR cell counter using the trypan blue exclusion method. Gray bars, cultured without MSCs; black bars, cultured with MSCs. MSCs were treated with IACS-010759 for 72 hours in single-culture conditions. (B) Adhesion of OCI-AML3 cells to cocultured MSCs. OCI-AML3 cells were cultured on MSCs for 48 hours with or without IACS-010759 (30 nM). Adherent cells were counted as described in the supplemental Materials and Methods. (C) The OCR was measured by extracellular flux assay in OCI-AML3 and MOLM13 cells treated with IACS-010759 (30 nM) with or without MSCs for 2 hours. Cocultured AML cells were separated from the MSC monolayer by careful pipetting before the extracellular flux assay. A total of 5×10^5 cells per well were used. Three technical replicates for each condition were plated. During the assay, oligomycin (Oligo), carbonyl cyanide-p-trifluoromethoxyphenylhydrazone (FCCP), rotenone, and antimycin A were added according to the manufacturer's instructions as described in the supplemental Materials and Methods. Representative of the results from 3 independent Cell Mito Stress Tests, and calculated values for the baseline OCR (indicated by the arrow) are shown. Comparisons of the reductions in OCR by treatment with IACS-010759 (IACS)

Table 1. Clinical characteristics of patients with AML whose samples were used for CAGE analysis

Patient No.	IACS-010759 sensitivity	Diagnosis	% Blast	Mutation status
1	Sensitive	AML	78	*NRAS*
2	Sensitive	AML	74	*CEPBA; BCR-ABL1, E1A2*
3	Sensitive	AML	93	*FLT3*-ITD, *IDH1, NPM1*
4	Sensitive	AMOL	76	*DNMT3A, IDH1, NPM1, FLT3-D835+V491L*
5	Sensitive	AML	19	*EZH2, KRAS, NPM1, TET2, RUNX1*
6	Sensitive	AML	52	*FLT3-D835, NPM1*
7	Sensitive	AML	96	*NRAS, TET2, AML1-ETO*
8	Sensitive	AML	64	*GATA2, CEPBA*
9	Sensitive	AML	94	*FLT3-D835, IDH2, RUNX1, WT1*
10	Sensitive	AML	22	*ASXL1, GATA1, JAK2*
11	Sensitive	AML	87	*CEPBA, FLT3*-ITD, *WT1*
12	Sensitive	AMOL	73	*IDH2, NPM1*
13	Sensitive	AML	58	*DNMT3A, NRAS, TET2*
14	Sensitive	AML	15	*ASXL1, IDH1, JAK2*
15	Sensitive	AML	23	*CEPBA, ASXL1, EZH2, TET2*
16	Sensitive	AML	88	*FLT3*-ITD, *WT1*
17	Resistant	AMML	21	*IDH1, DNMT3A, NPM1, NRAS*
18	Resistant	AML	18	Negative
19	Resistant	AML	90	*NRAS*
20	Resistant	AML	80	*DNMT3A, JAK2, KIT, NRAS, RUNX1, TET2, WT1*
21	Resistant	AML	34	Negative
22	Resistant	AML	74	*RUNX1, TET2, TP53*
23	Resistant	AML	26	*FLT3-D835, NRAS*
24	Resistant	AMML	17	*TP53*
25	Resistant	AML	81	*IDH1, NOTCH1, TP53*
26	Resistant	AMOL	90	*DNMT3A, NPM1, NRAS, TET2*

AMML, acute myelomonocytic leukemia; AMOL, acute monoblastic leukemia; ITD, internal tandem duplication.

dual-positive cells was increased in OCI-AML3 cells, but not in OxPhosi-resistant MOLM13 cells (Figure 2A, right panel). In U937 cells with intermediate sensitivity to IACS-010759, treatment with IACS-010759 modestly increased the fraction of dsRed-positive cells (control, 0.3% ± 0.2% vs MSC coculture, 2.7% ± 1.3%; $P = .008$) (supplemental Figure 5). These results indicate that metabolic stress in OxPhos-dependent cells can induce the transfer of MSC mitochondria into leukemia cells.

To further characterize the direct interactions between OCI-AML3 cells and MSCs, coculture was performed with and without transwell inserts. Figure 2B shows that dual-positive cells were apparent only when the cells were cocultured without separating filters. We then performed flow cytometric analysis to identify dsRed fluorescence derived from MSC mitochondria in OCI-AML3 cells that adhered to MSCs after treatment with IACS-010759. As shown in Figure 2C, the rate of transfer of MSC-derived mitochondria in adherent OCI-AML3 cells was significantly increased by OxPhos inhibition, but this increase was not observed in single-culture conditions.

To investigate how the mitochondria were transferred, we carefully examined the microscopic images at high magnification. The snapshots in Figure 2D (upper panels) show OCI-AML3 cells with green fluorescence and an MSC with red fluorescence connected by very thin tubes that resemble TNTs, which are actin-containing membrane protrusions that play an essential role in long-range intercellular communication. Small red particles were seen inside some of these tubes, which might be the migrating mitochondria. However, in other cases,

Figure 1. (continued). between the single-culture condition and MSC coculture condition are shown on the right. (D) OCR was measured by extracellular flux assay in MSCs treated with IACS-010759 (30 nM) for 2 hours. A total of 6×10^4 cells per well were used. Three technical replicates for each condition were plated. During the assay, oligomycin, FCCP, rotenone, and antimycin A were added according to the manufacturer's instructions. Representative Cell Mito Stress Test results (n = 3), and calculated values for the baseline OCR (indicated by the arrow) are shown. (E-F) OCI-AML3 cells were treated with 20 nM or 30 nM IACS-010759 for 72 hours in the presence or absence of MSCs. Nonadherent OCI-AML3 cells were separated from the MSC monolayer by careful pipetting. OCI-AML3 cells that adhered to MSCs were separated from cocultured MSCs by magnetic-activated cell sorting (MACS) using anti-CD45 microbeads after trypsinization as described in panel E (supplemental Materials and Methods) or (F) separated by the transwell insert into upper and lower compartments. Apoptosis of treated cells was detected by staining with annexin V-fluorescein isothiocyanate (FITC)/propidium iodide (PI) and an anti-CD45 allophycocyanin (APC)-conjugated antibody using flow cytometry. Representative flow cytometry plots showing annexin V (x-axis) and PI (y-axis) staining are shown on the right . Error bars in the graphs show the means ± SDs of the results from 3 independent experiments. *$P < .05$; **$P < .01$.

Table 2. Differently expressed promoters in OxPhosi-resistant and OxPhosi-sensitive primary AML cells from peripheral blood

Gene	Fold change (log_2 >2.0)	*P*	FDR <0.05	Adhesion	Migration	Actin cytoskeleton dynamics
Higher in OxPhosi-resistant than OxPhosi-sensitive cells						
C2CD4B	6.788	3.67E-07	0.0082	●		
VPREB3	6.292	6.13E-07	0.0095			
PHLDB1	6.192	2.85E-06	0.0213	●		
FXYD2	5.739	3.44E-06	0.0231	●		●
CAMP	5.354	9.09E-07	0.0131	●		●
TRIO	5.021	2.26E-06	0.0196	●	●	●
SASH1	4.479	1.25E-05	0.0467		●	
LCN6	4.366	2.27E-06	0.0196	●		●
RET	4.188	1.93E-07	0.0080		●	●
TCN1	3.773	1.22E-05	0.0466	●		
RCBTB2	3.660	2.85E-07	0.0082	●		●
UBR4	3.591	3.14E-06	0.0218			
FSTL3	3.588	7.06E-06	0.0353	●		●
CXCR1	3.539	4.22E-06	0.0258	●	●	●
RASL11A	2.623	4.64E-07	0.0094	●	●	●
FAM55C	2.353	7.34E-06	0.0353	●		●
Lower in OxPhosi-resistant than in OxPhosi-sensitive cells						
CXCL5	−8.746	5.87E-06	0.0312		●	
IGLV5-37	−6.941	1.03E-05	0.0438			
IRX1	−6.795	2.15E-06	0.0196	●		
PCDH10	−6.240	2.00E-07	0.0080			
HOXB9	−6.068	8.89E-06	0.0408			
COL14A1	−6.028	2.53E-06	0.0196	●		
GLIS3	−5.496	5.64E-06	0.0309			
ZNF385C	−5.156	2.40E-06	0.0196			
PLEKHA5	−4.512	2.38E-07	0.0080			
CMAHP	−3.406	2.04E-07	0.0080			
ANKRD36B	−2.598	1.19E-06	0.0160			
TPTEP1	−2.475	1.03E-05	0.0438			

we observed much thicker tubing and protrusions from AML cells and green, but not red, fluorescence in the tubing (Figure 2D, lower panel). These morphologic changes could be associated with the transcriptional upregulation of genes associated with adhesion and rho GTPase, which are involved in TNT formation through actin polymerization and which were detected by CAGE analyses. Electron microscopy further revealed that treatment with IACS-010759 induced the transport of mitochondria to the leading edge of the protrusions of OCI-AML3 cells adhering to cocultured MSCs; this was not evident in untreated OCI-AML3 cells (Figure 2E).

ICAM-1 mediates the transfer of mitochondria from MSCs to AML cells

Previous studies demonstrated that oxidative stress induced by chemotherapeutic agents can trigger the formation of cell adhesion-induced TNTs. Specifically, ICAM-1 can mediate the transfer of mitochondria between leukemia cells and MSCs.[9-11,28] Indeed, we found that inhibition of ICAM-1 with a neutralizing antibody (Figure 3A, left panel) and blockade of actin polymerization with cytochalasin D (Figure 3A, right panel) blocked the transfer of MSC-derived mitochondria to OCI-AML3 cells. We further observed that the blockade of mitochondrial transfer induced by inhibition of ICAM-1 and actin polymerization increased the cytotoxic effects of OxPhos inhibition (Figure 3B). Because CAGE and extracellular flux analyses indicated that the AML cell adhesion to MSCs is critical for acquired resistance to OxPhos inhibition by reversing metabolic suppression, we investigated the changes in energy metabolism in AML cells after blockade of ICAM-1. An extracellular flux assay demonstrated that the ICAM-1 neutralizing antibody did not affect OCR by itself; instead, it significantly enhanced the metabolic suppression induced by IACS-010759 in OCI-AML3 cells cocultured with MSCs (Figure 3C).

Although vascular cell adhesion molecule-1 (VCAM-1) plays a role in the binding of leukemia cells through α4β1-integrin,[29-31] the anti-α4β1 integrin antibody natalizumab[32] did not inhibit mitochondrial transfer induced by OxPhos inhibition (supplemental Figure 6). In addition, it has been reported that mitochondrial uptake can occur through endocytosis.[11] However, the endocytosis inhibitor dansylcadaverine,

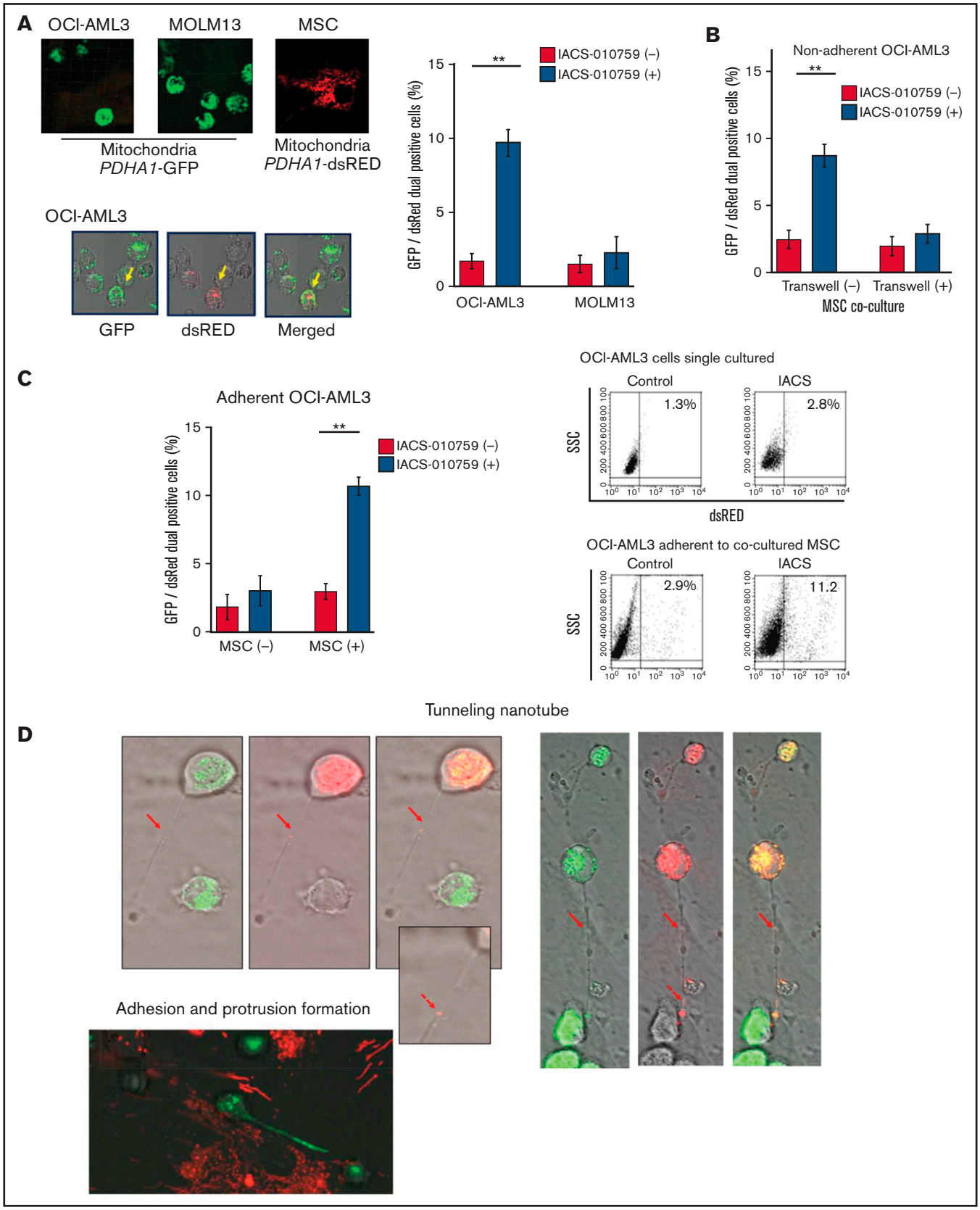

Figure 2.

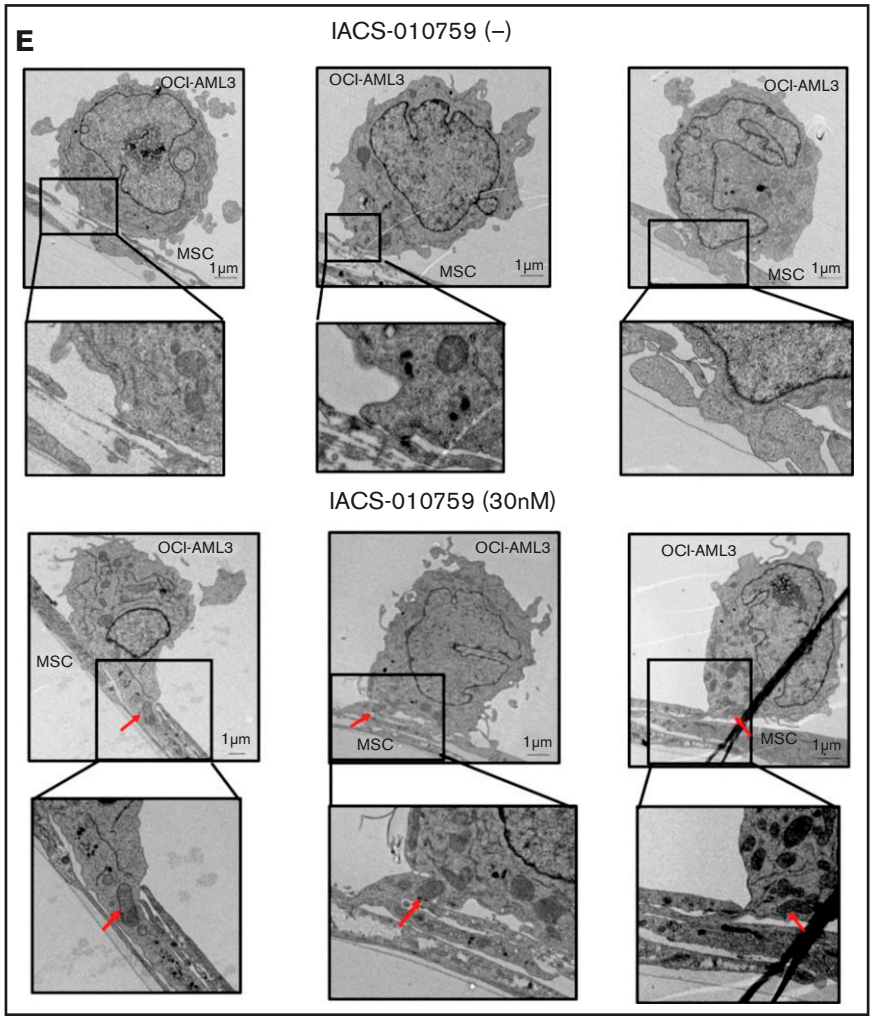

Figure 2. Mitochondrial transfer from MSCs to AML cells is induced by OxPhos inhibition. (A) OCI -AML3 and MOLM13 cells were stably transfected with mitochondria-targeted *PDHA1*-GFP, and MSCs were transfected with *PDHA1*-dsRed (upper left panel). Confocal microscopy images at ×40 magnification. Representative confocal images of dual fluorescence (GFP and dsRed)–positive OCI-AML3 cells cocultured with MSCs in the presence of 30 nM IACS-010759 for 72 hours (lower left panel; yellow arrow: GFP and dsRed dual-positive cell). To quantitatively determine the rate of mitochondrial transfer, OCI-AML3 cells cocultured with MSCs were separated from the MSC monolayer by careful pipetting, and the GFP and dsRed dual-positive recipient cells per 100 GFP^+ cells ($n > 5$) were counted at ×40 magnification by live-cell imaging with confocal microscopy (right panel). Laser scanning was used to obtain images under a confocal microscope. (B) To compare direct-contact to noncontact conditions, OCI-AML cells were cocultured with *PDHA1*-dsRed–transfected MSCs in direct contact or separated by a transwell insert and treated with IACS-010759 (30 nM) for 72 hours. OCI-AML3 cells cultured in direct-contact conditions were separated from the MSC monolayer by careful pipetting. dsRed-positive OCI-AML3 cells per 100 OCI-AML3 cells ($n > 5$) were counted at ×40 magnification by live-cell imaging with confocal microscopy. (C) *PDHA1*-GFP–transfected OCI-AML3 cells were treated with the OxPhosi IACS-010759 (30 nM) for 72 hours in the presence or absence of *PDHA1*-dsRed transfected MSCs. The rate of MSC-derived mitochondrial transfer in OCI-AML3 cells that adhered to MSCs was determined by flow cytometric analysis after depletion of MSCs with MACS as described in supplemental Materials and Methods. Representative flow cytometry plots are shown on the right . (D) Representative confocal microscopy images show the formation of TNTs and protrusion formation in OCI-AML3 cells after treatment with IACS-010759 under MSC coculture conditions. The red arrows indicate the transfer of MSC-derived mitochondria along TNTs. Confocal microscopy images at ×63 magnification. (E) OCI-AML3 cells were treated with the OxPhosi IACS-010759 (30 nM) for 48 hours in the presence of MSCs. Representative electron microscopy images show the IACS-010759–treated OCI-AML3 cells migrating to cocultured MSCs with mitochondrial transport to the leading edge of a protrusion, which was not observed in untreated (control) cells. Red arrows indicate mitochondria. Error bars in the graphs show the means ± SDs of the results from 3 independent experiments. $^{**}P < .01$. SSC, side scatter.

which blocks macrovesicle endocytosis, failed to inhibit the transfer of mitochondria (supplemental Figure 7).

OxPhos inhibition increases the functional mitochondria in OCI-AML3 cells cocultured with MSCs

Under stress conditions induced by chemotherapeutic drugs or OxPhos inhibition, a dynamic increase in mitochondrial fission was reported to segregate damaged mitochondria and maintain functional mitochondria.[28-32] Electron microscopy showed that treatment with an OxPhosi indeed induced mitochondrial fission in leukemia cells, as evidenced by increased numbers of mitochondria in OCI-AML3 cells cocultured with MSCs (Figure 4A; supplemental Figure 8). As shown in Figure 4B, the mtDNA copy numbers in OCI-AML3 cells (mtDNA:nuclear DNA ratio) were significantly increased by OxPhos inhibition under MSC coculture conditions but not in monoculture.

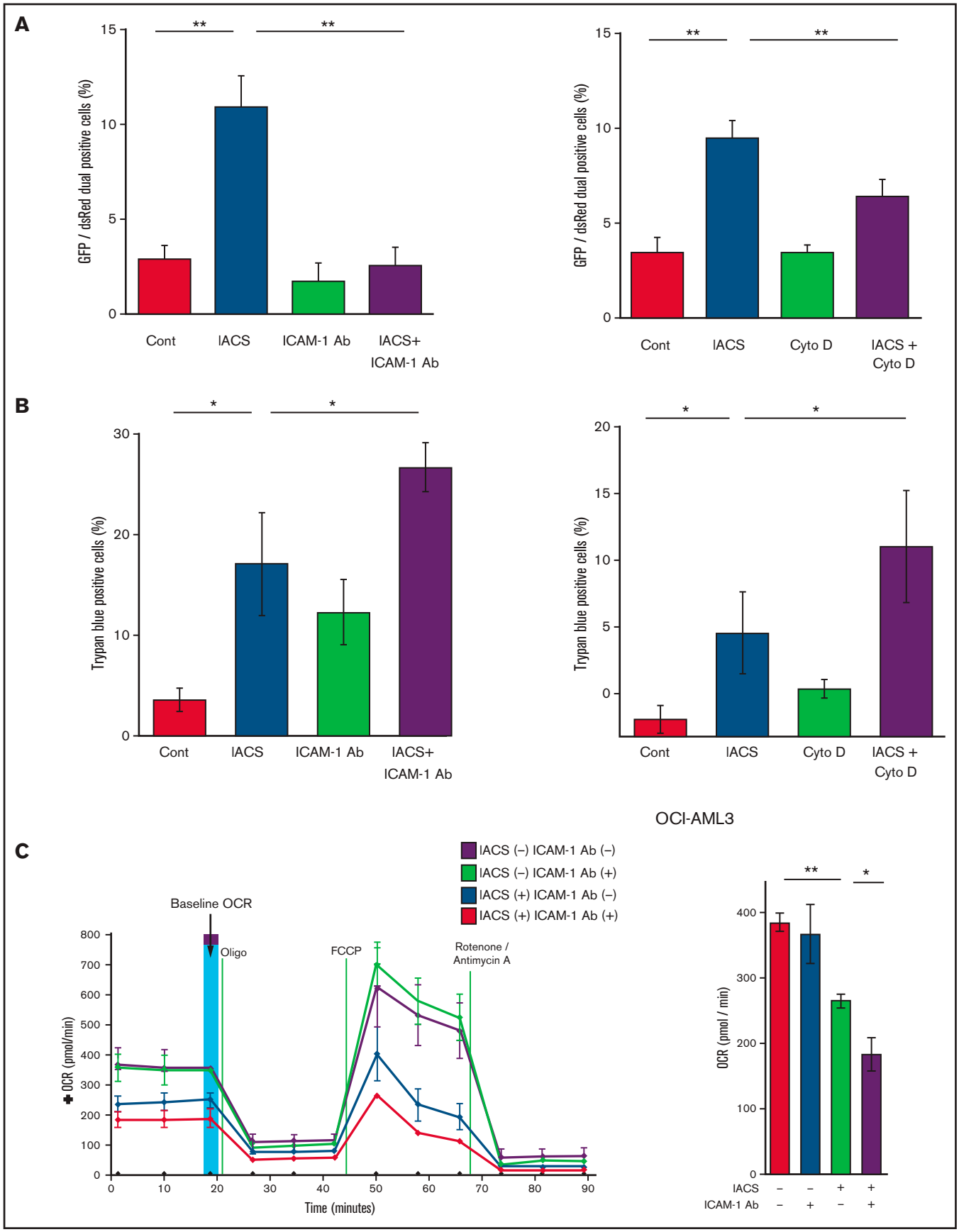

Figure 3.

These results indicate that OxPhos inhibition increases the number of mitochondria in AML cells coexisting with BM stromal cells.

Next, we measured the mitochondrial membrane potential to assess mitochondrial function using the membrane-permeant JC-1 dye. The JC-1 dye enters the cell and accumulates in the mitochondria. In energized and negatively charged mitochondria, JC-1 spontaneously forms red fluorescent J-aggregates. In damaged mitochondria with collapsed membrane potential, JC-1 retains its original green fluorescence as a monomer. As shown in Figure 4C, coculture of OCI-AML3 cells with MSCs facilitated a moderate increase in the ratio of aggregated JC-1 with red fluorescence to monomer JC-1 with green fluorescence, which reflects an increase in the energized mitochondria with intact membrane potential compared with damaged mitochondria with collapsed membrane potential. OxPhos inhibition further increased levels of aggregated JC-1 under MSC coculture conditions. The fluorescent images of merged aggregated JC-1 (red) and monomer JC-1 (green) are shown in supplemental Figure 9. These findings indicate that in addition to direct mitochondrial transfer, mitochondrial fission in AML cells results in a net increase in the number of total and functional mitochondria that dampen the response of AML cells to inhibition by OxPhos in the BM microenvironment. To identify the role of AML cell adhesion to BM stromal cells in regulating the number of mitochondria, further investigations are warranted, including direct observation and measurement of mitochondria by electron microscopy with or without a transwell inserts.

OxPhos inhibition increases ROS generation and mitophagy in OCI-AML3 cells cocultured with MSCs

Because mitochondrial fission is known to be triggered by generation of ROS, we measured total ROS production. Inhibition of OxPhos induced significant upregulation of ROS production in OCI-AML3 cells cocultured with MSCs (Figure 5A). During ROS production and mitochondrial fission, defective mitochondria are commonly removed by mitophagy (the selective degradation of mitochondria by autophagy[33]), which is important in cellular metabolism and is essential for cell survival.[34,35] We observed that OxPhos inhibition induced autophagy, with conversion of LC3-I to LC3-II in both monoculture and MSC coculture, but more prominently in MSC coculture. This effect was enhanced by the lysosome inhibitor bafilomycin (Figure 5B). Indeed, the number of cells that were positive for a dye that detects damaged mitochondria fused to lysosomes (ie, mitophagy) was significantly increased in OCI-AML3 cells treated with an OxPhosi in both monoculture and coculture with MSCs but more prominently in those cocultured with MSCs (Figure 5C). Figure 5D shows representative electron microscopy images of MSC-derived *PDHA1*-dsRED-positive mitochondria immunolabeled with gold particles and wrapped in an autophagosome in cocultured OCI-AML3 cells.

OxPhos inhibition combined with cytarabine increases mitochondrial transfer from MSCs and inhibits apoptosis induction in OCI-AML3 cells

We further observed that coculture of OCI-AML3 cells with MSCs inhibited the apoptosis-inducing effect of the combination of low-dose cytarabine and OxPhos inhibition. As shown in Figure 6A, induction of apoptosis by the combination of cytarabine and IACS-010759 was reduced by the MSC coculture, more prominently in MSC-adherent OCI-AML3 cells than in nonadherent cells.

We then investigated whether the mitochondrial transfer from MSCs to OCI-AML3 cells triggered by OxPhos inhibition was further enhanced by co-treatment with low-dose cytarabine. Using OCI-AML3 cells transfected with *PDHA1*-GFP and MSCs transfected with *PDHA1*-dsRed, we observed by confocal microscopy, that treatment with cytarabine plus OxPhosi increased the transfer of MSC-derived mitochondria to cocultured OCI-AML3 cells that were not adherent to MSC layers (Figure 6B; supplemental Figure 10). Flow cytometric analysis of dsRed fluorescence in OCI-AML3 cells cocultured with MSCs also demonstrated an increase of dsRed-positive OCI-AML3 cells, indicating mitochondrial transfer from MSCs (Figure 6C). Taken together, these findings indicate that BM stromal cells abrogate the apoptotic effects of cytarabine plus OxPhos inhibition in AML cells and that mitochondrial transfer triggered by OxPhos inhibition might be at least in part responsible for this resistance.

In vivo transcriptome analysis of OxPhosi-resistant AML cells

We examined gene promoter expression of OxPhosi-sensitive and -resistant AML PDXs by CAGE analysis. Primary AML cells from 7 AML PDXs (Table 3) were injected into irradiated NSG mice, which were randomly assigned upon documented engraftment to receive IACS-010759 or vehicle (n = 3 mice per group). The antileukemia efficacy of the treatment was monitored by serial measurements of circulating AML cells as described in the supplemental Materials and Methods. Of the 7 models tested, we defined 3 PDXs as sensitive and 4 as resistant to ongoing therapy with OxPhosi(s) (Figure 7).

In the resistant models, CAGE analysis of OxPhosi-induced changes (comparing pre- and posttreatment) identified upregulation of 100 promoters and downregulation of 218 promoters (FDR, <0.05; $\log_2$ fold change, >2.0 by EdgeR), including notably increased promoter

Figure 3. Blockade of ICAM-1 and actin polymerization inhibits mitochondrial transfer and increases cytotoxic effects of OxPhos inhibition. (A-B) *PDHA1*-GFP–transfected OCI-AML cells were cocultured with *PDHA1*-dsRed–transfected MSCs with or without IACS-010759 (30 nM) and/or an ICAM-1 neutralizing antibody (Ab) (25 μg/mL) (left) or cytochalasin D (Cyto D) (350 nM) (right). (A) To quantitatively determine the rate of mitochondrial transfer, the number of GFP and dsRed dual-positive recipient cells per 100 GFP^+ cells was counted at ×40 magnification by live-cell imaging with confocal microscopy. Laser scanning was used to obtain images under a confocal microscope. To quantitatively determine the rate of mitochondrial transfer, OCI-AML3 cells cocultured with MSCs were separated from the MSC monolayer by careful pipetting, and the GFP and dsRed dual-positive recipient cells per 100 GFP^+ cells were counted at ×40 magnification by live-cell imaging with confocal microscopy (right panel). Laser scanning was used to obtain images under a confocal microscope. The means ± SDs of the results from 5 independent experiments. (B) The percentage of dead cells was determined by the trypan blue exclusion method. (C) The OCR was measured by extracellular flux assay in OCI-AML cells cocultured with MSCs with or without IACS-010759 (20 nM) and/or an ICAM-1 neutralizing antibody (25 μg/mL). Cocultured OCI-AML3 cells were separated from the MSC monolayer before the extracellular flux assay. A total of 5×10^5 AML cells were added per well. Three technical replicates for each condition were plated. During the assay, oligomycin, FCCP, rotenone, and antimycin A were added according to the manufacturer's instructions. Representative of the results from 3 independent Cell Mito Stress Tests, and calculated values for the baseline OCR (indicated by the arrow) are shown. Error bars in the graphs show the means ± SDs of the results from 3 independent experiments. Two-way analysis of variance $^*P < .05$; $^{**}P < .01$. Cont, control.

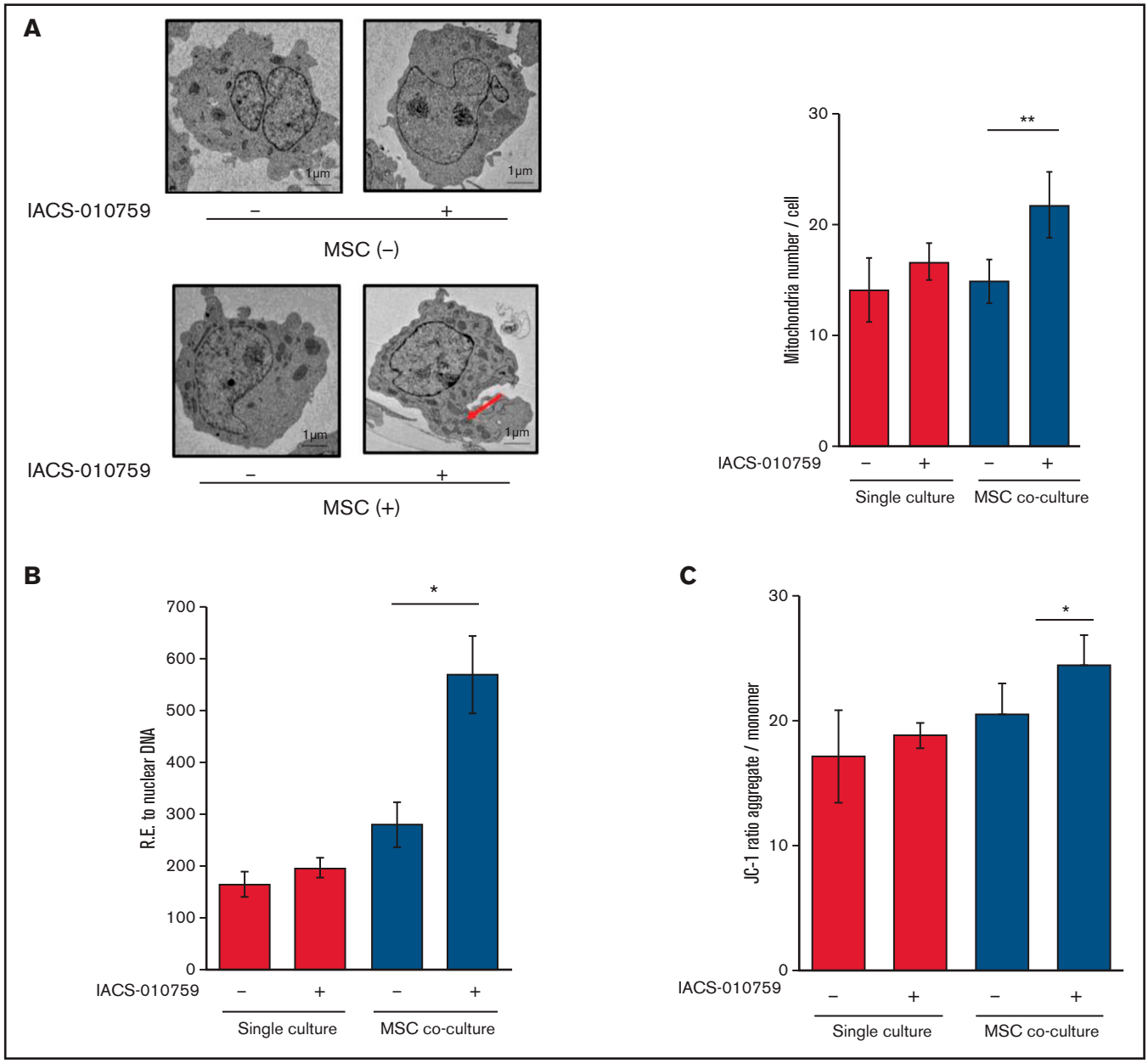

Figure 4. OxPhos inhibition increases the number of functional mitochondria in OCI-AML3 cells cocultured with MSCs. (A) OCI-AML3 cells were treated with the OxPhosi IACS-010759 (30 nM) for 72 hours with or without cocultured MSCs. Representative electron microscopy images showing the increased numbers of small mitochondria in IACS-010759–treated OCI-AML3 cells cocultured with MSCs (left panel). The number of mitochondria inside OCI-AML3 cells was counted in more than 10 image fields at ×40 magnification by live-cell imaging with confocal microscopy. (B) Mitochondrial DNA copy number was assessed by quantitative polymerase chain reaction. Mitochondrial DNA content was normalized to nuclear DNA content. Data are presented as the mean of 3 independent experiments. (C) OCI-AML3 cells were treated with IACS-010759 (30 nM) for 4 hours with or without cocultured MSCs. The JC-1 monomer with green fluorescence reflects mitochondria with collapsed membrane potentials, and aggregated JC-1 with red fluorescence reflects mitochondria with intact membrane potentials. The ratio of the red and green optical density is shown. Data are presented as the means of 3 independent experiments. Error bars in the graphs show the means ± SDs of the results from 3 independent experiments. *$P < .05$; **$P < .01$.

expression (log_2 fold change, >3.0) of genes associated with adhesion (*SORBS2*,[36] *CCR8*,[37] *BAI2*,[38] *LAG3*,[39] *PLXDC1*,[40] *CD200R1*,[41] and *ATN1*[42]), migration (*CCR8*,[43] *PLXDC1*,[44] *COBLL1*,[45] and *SIGIRR*[46]), and actin cytoskeleton dynamics (*BMF*,[47] *BEST1*,[48] *TNNT3*,[49] and *FGD1*[50]) (Table 4). We further observed significant upregulation of promoter expression of *ASS1*, which encodes argininosuccinate synthase 1 and is responsible for the biosynthesis of arginine[51,52]; of *LRP1*, which encodes low-density lipoprotein receptor–related protein-1 (LRP1), a member of the low-density lipoprotein receptor family involved in lipid homeostasis[53]; *MRPS2*, encoding mitochondrial ribosomal protein S2[54]; and *PDE9A*, encoding phosphodiesterase 9A, which catalyzes the hydrolysis of cyclic adenosine 3′,5′-monophosphate (cAMP) and cyclic guanosine 3′,5′-monophosphate (cGMP).[55] DEGseq detected 247

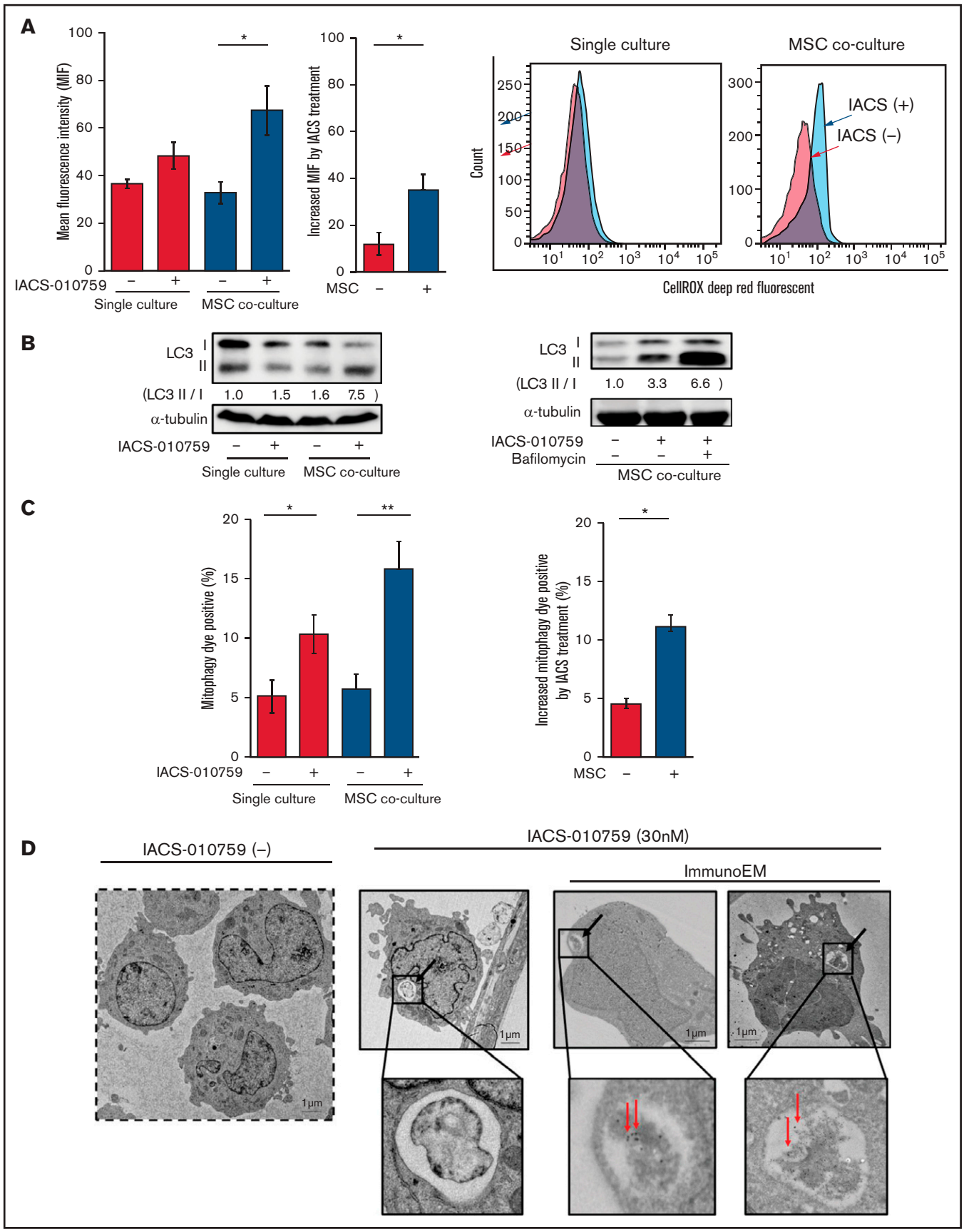

Figure 5.

gene promoters that were upregulated and 925 promoters that were downregulated by treatment with OxPhosi in all 4 OxPhosi-resistant PDX mouse models (supplemental Table 2). Notably, 5 of the adhesion-associated promoters that were consistently upregulated by OxPhos inhibition in the 4 resistant mouse models (*CCR8, BAI2, LAG3, PLXDC1,* and *ATN1*) were unchanged or downregulated in the 3 sensitive models (Table 5).

We further investigated the uptake of murine mtDNA into the human AML PDX cells in vivo using the Mouse Feeder Cell Quantification Kit (Takara Bio; supplemental Materials and Methods). Although murine nuclear DNA measurements were negative in AML cells, we detected murine mtDNA in both AML PDXs treated with IACS-010759. In OxPhosi-resistant AML PDX #31 treated with IACS-010759, the ratio of murine mtDNA to human nuclear DNA was higher than in OxPhosi-sensitive PDX #28 (3.0 vs 0.1) (Figure 7; supplemental Table 3).

Discussion

In this study, we discovered a novel role of BM stromal cells: that of promoting the resistance of AML cells to the metabolic stress of OxPhos inhibition. Our findings indicate that the OxPhos-dependent AML cells become less responsive to OxPhos inhibition while receiving mitochondria from MSCs, and in parallel, they stimulate endogenous mitochondrial fission as an anaplerotic reaction and eliminate damaged mitochondria by mitophagy, all contributing to AML survival.[35]

Tumor cells have been shown to obtain new DNA from surrounding stromal cells via the formation of TNTs,[56,57] gap junctions,[58] and endocytosis.[11] The horizontal transfer of mtDNA from host cells in the tumor microenvironment to tumor cells is known to re-establish respiration and increase tumor-initiating efficacy in in vivo models.[59]

We observed that the additive apoptosis-inducing efficacy of the OxPhosi(s) IACS-010759 and cytarabine in AML cells was abrogated under MSC coculture conditions in parallel with reduced OxPhos inhibition and increased mitochondrial transfer from MSCs to AML cells. These findings are supported by the recent study of Farge et al,[60] which indicates the key role of high OxPhos in cytarabine resistance. Cytarabine has been shown to inhibit DNA polymerase gamma, which is involved in mtDNA synthesis, leading to the production of ROS and the damage of oxidative mtDNA.[61] In turn, it has been reported that cytarabine-induced ROS induces mitochondrial migration from MSCs to leukemic cells via cell adhesion and/or TNTs.[10,28] These results indicate that MSCs provide a direct compensatory effect by supplying mitochondria to OxPhosi-sensitive AML cells with low endogenous OxPhos.

Regarding the mechanisms of TNT formation, an active process based on the extension of a filopodium-like protrusion from one cell to another has been proposed.[62] Contact-dependent intercellular transfer requires activation of motor proteins such as rho GTPases that positively regulate formation of TNTs through actin polymerization[63,64] and formation of filopodia through focal adhesion.[65] Recently, a transmembrane complex gap junction channel, connexin 43, was shown to open up under conditions of ROS-induced oxidative stress via activation of PI3K-Akt, which enables mitochondrial transfer from BM stromal cells to hematopoietic stem cells.[66] Further investigations are required to identify the role of gap junctions in the regulation of TNT formation, mitochondrial trafficking and the protective effects of the leukemic niche.

This study also demonstrated that OxPhos inhibition under MSC coculture conditions stimulates mitochondrial fission and increases functional mitochondria in AML cells. Mitochondrial fission in which damaged mitochondria are segregated[67-71] is commonly associated with mitophagy, the selective removal of mitochondria by autophagy.[33] Efficient mitophagy is important in cellular metabolism and is essential for cell survival.[34,35] Of note, we observed that the MSC-derived mitochondria transferred to AML cells were degraded inside autophagosomes in AML cells. This finding is consistent with a recent study reporting that the mitochondria transferred from MSCs to corneal endothelial cells via TNTs were degraded by lysosomes in recipient cells.[72] These observations indicate the possibility of another important mechanism for maintaining mitochondrial function, but its causal relationship with treatment resistance is left to further study.

One limitation of our coculture experiments is that the cocultured MSCs were exposed to IACS-010759 together with AML cells, and this treatment affects both cell types. However, MSCs undergo less pronounced inhibition of OCRs with IACS-010759 than AML cells, which indicates that the mitochondrial damage to MSCs is less than that in AML cells. Leukemia stem cells (LSCs) are characterized by a low rate of energy metabolism[5] and an inability to upregulate glycolysis after OxPhos inhibition, which increases their sensitivity to OxPhos blockade.[73] At the same time, LSCs undergo more mitochondrial fission and mitophagy than do bulk AML cells, and they must balance mitochondrial functions such as bioenergetics, ROS generation, and apoptosis to maintain their stemness.[71] Because the mitochondrial network is known to be fragile in LSCs, combination therapies with blockade of other metabolic pathways might be a strategy to overcome the BM microenvironment–induced resistance to OxPhos inhibition.

We also observed an increase in promoter expression of the amino acid and lipid metabolism–related genes *ASS1* and *LRP1* in

Figure 5. OxPhos inhibition induces ROS and mitophagy in OCI-AML3 cells cocultured with MSCs. (A) Summary data (left) and representative flow cytometry histograms (right) showing ROS production in OCI-AML3 cells treated with the OxPhosi IACS-010759 (30 nM) for 72 hours with or without cocultured MSCs. Comparisons of the increase in ROS by treatment with IACS-010759 (IACS) between the single-culture condition and MSC coculture condition are shown in the middle. An increase in relative fluorescence is reflected by a rightward shift along the x-axis of the histograms. (B) Cells were treated with IACS-010759 (30 nM) for 18 hours in the absence or presence of the lysosomal inhibitor bafilomycin A1 (10 μM), and cell lysates were examined by immunoblotting. LC3-II protein levels were normalized to LC-I levels to determine the differences in protein expression between the cells cultured with and without MSCs. (C) Uptake of mitochondria by lysosomes was evaluated by mitophagy assay. Comparisons of the increase in mitophagy dye positivity by treatment with IACS-010759 between the single-culture condition and MSC coculture condition are shown on the right. (D) Representative immunoelectron microscopy images showing MSC-derived mitochondrial fragments inside autophagosomes in cocultured OCI-AML3 cells. OCI-AML3 cells were cocultured with *PDHA1*-dsRed–transfected MSCs and treated with 30 nM IACS-010759. Electron microscopy images at ×2000 magnification. Fixed sections were immunolabeled with gold as described in supplemental Materials and Methods. Black arrows indicate mitophagy; red arrows indicate MSC-derived mitochondrial fragments surrounded by autophagosomes. Error bars in the graphs show the means ± SDs of 3 independent experiments. *$P < .05$; **$P < .01$.

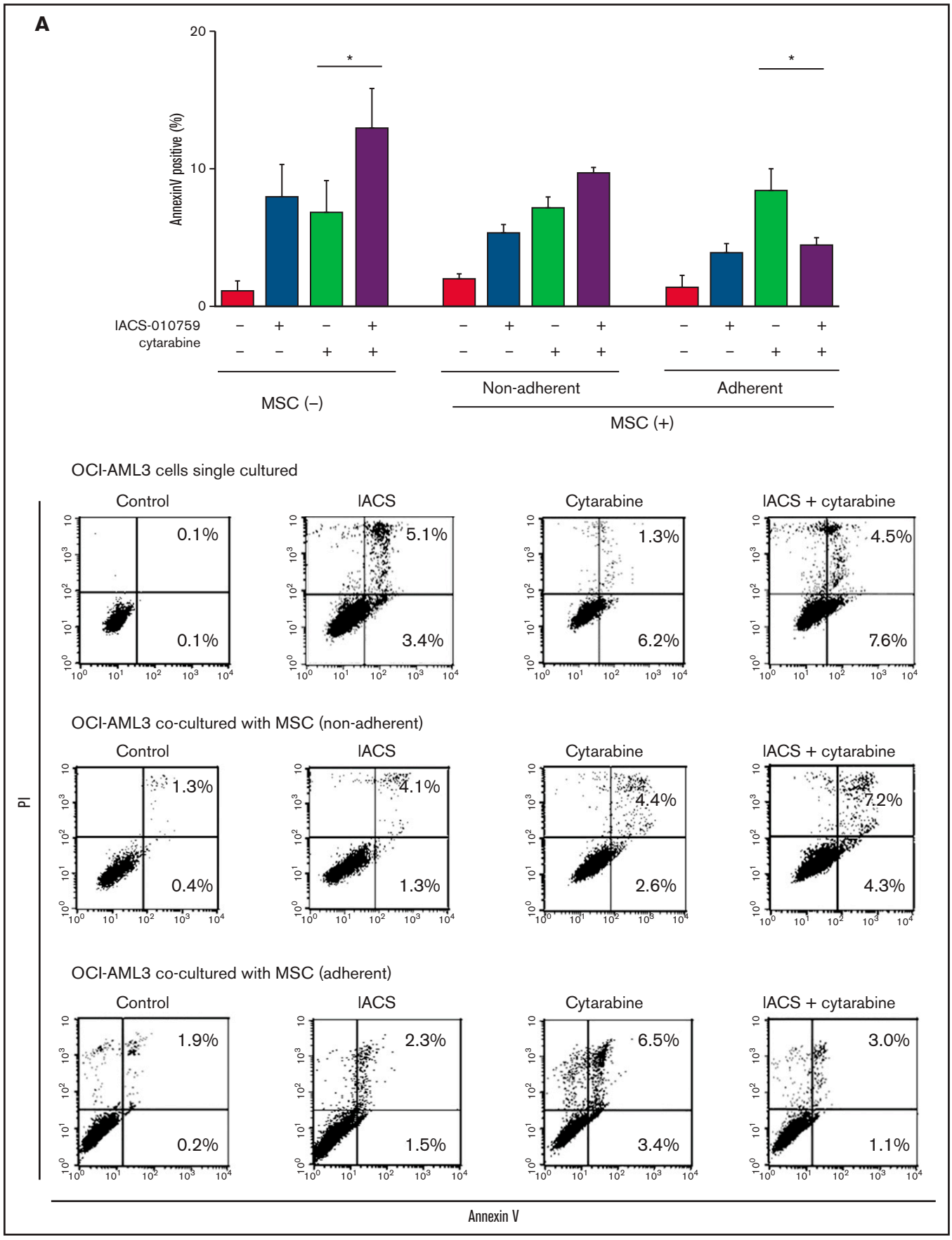

Figure 6.

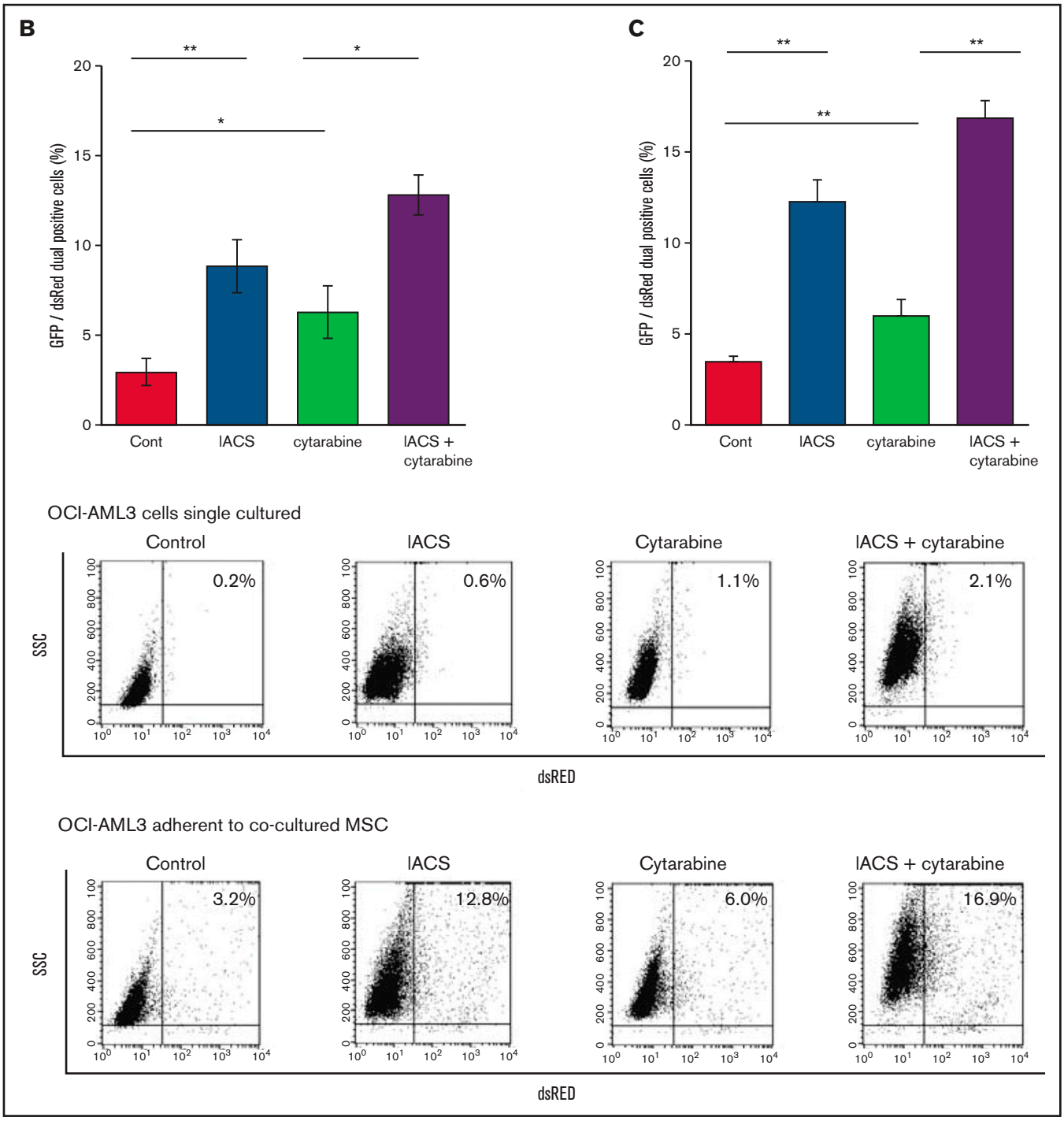

Figure 6. MSC coculture inhibits OxPhos inhibition and cytarabine-induced apoptosis with increasing mitochondrial transfer. OCI-AML3 cells were treated with OxPhosi IACS-010759 (20 nM) and/or cytarabine (500 nM) for 72 hours in the presence or absence of MSCs. In cocultured cells, nonadherent OCI-AML3 cells were separated from the MSC monolayer by careful pipetting. After removing nonadherent cells, the OCI-AML3 cells that adhered to cocultured MSCs were trypsinized with MSCs and then separated from MSCs by magnetic-activated cell sorting using anti-CD45 microbeads. (A) Apoptotic cell death of adherent and nonadherent OCI-AML3 cells in single-culture and MSC-coculture conditions was detected by staining with annexin V-FITC/PI and an anti-CD45 APC-conjugated antibody using flow cytometry. Representative flow cytometry plots (bottom) show annexin V (x-axis) and PI (y-axis) staining. (B) The rate of MSC-derived mitochondrial transfer in cocultured nonadherent OCI-AML3 cells was detected by counting the number of GFP and dsRed dual-positive recipient cells per 100 GFP^+ cells ($n > 5$) at ×40 magnification by live-cell imaging with confocal microscopy using laser scanning to obtain images. (C) The rate of MSC-derived mitochondrial transfer in OCI-AML3 cells that adhered to MSCs was detected by flow cytometric analysis after depletion of MSCs with MACS as described in supplemental Materials and Methods. Representative flow cytometry plots are shown (right). Error bars in the graphs show the means ± SDs of the results from 3 independent experiments. Two-way analysis of variance (ANOVA) *$P < .05$; **$P < .01$.

Table 3. Clinical characteristics of patients with AML whose samples were used for in vivo experiments

Patient No.	OxPhosi sensitivity	Diagnosis	Mutation status
27	Sensitive	AML	*FLT3*-ITD, *CEPBA*, *IDH1*, *NPM1*, *NRAS*
28	Sensitive	AML	*FLT3*-ITD, *DNMT3A*, *IDH1*, *KIT*, *NPM1*
29	Sensitive	AMML	*FLT3*-ITD, *IDH1*, *NPM1*
30	Resistant	AML	*FLT3*-ITD, *DNMT3A*, *NPM1*, *TP53*
31	Resistant	AML	*FLT3*-ITD, *DNMT3A*, *IDH2*, *NPM1*
32	Resistant	AML	*FLT3*-ITD, *DNMT3A*, *IDH1*, *NPM1*
33	Resistant	AML	*FLT3*-ITD, *DNMT3A*, *EGFR*, *IDH1*, *NPM1*, *TET2*

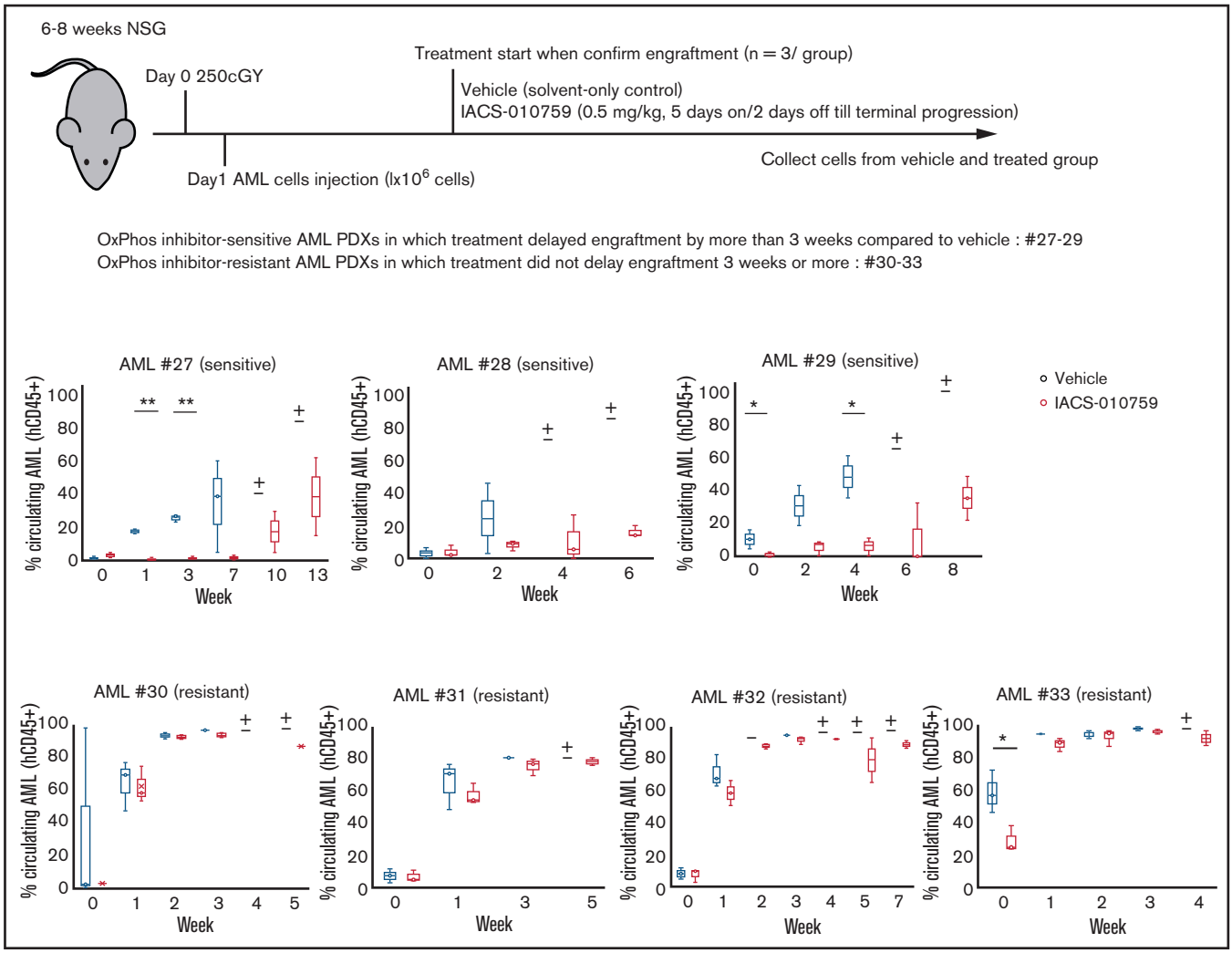

Figure 7. OxPhosi-resistant and OxPhosi-sensitive AML cells in mouse xenograft model. NOD-*scid* IL2Rγ^{null} (NSG) mice were injected with 1 million AML PDX cells 24 hours after receiving irradiation at 250 cGy. Mice were randomly assigned to receive vehicle or IACS-010759 (5.0 mg/kg; 5 days on/2 days off until terminal progression) (n = 3 mice per group). Engraftment of the leukemic cells in the peripheral blood was determined by flow cytometry with an anti-human CD45 antibody. OxPhosi-sensitive AML PDXs were from patients 27 to 29; OxPhosi-resistant AML PDXs were from patients 31 to 33. (+) Indicates that only 1 mouse survived . The thick horizontal lines in the bars represent median. Error bars in the graphs show means ± SDs. *$P < .05$; **$P < .01$.

Table 4. Upregulated promoters by OxPhosi treatment in OxPhosi-resistant AML cells in vivo

Gene name	Log_2 fold change	*P*	FDR	Adhesion	Migration	Actin cytoskeleton dynamics
Higher in OxPhosi-treated AML cells than in vehicle-treated cells						
BMF	5.518	1.39E-06	0.0002			●
SORBS2	5.348	7.92E-05	0.0050	●		
CCR8	4.640	2.67E-46	<0.0001	●	●	
BAI2	4.565	4.54E-04	0.0205	●		
PTPDC1	4.312	2.75E-04	0.0137			
GPR162	4.189	4.26E-07	0.0001			
MRPS2	4.158	1.02E-03	0.0387			
IGLV7-43	4.155	7.37E-04	0.0300			
LAG3	4.145	1.10E-03	0.0413	●		
TRAV21	3.970	1.33E-03	0.0481			
ASS1	3.904	1.11E-19	0.0000			
BEST1	3.534	7.29E-04	0.0298			●
PDE9A	3.492	5.08E-04	0.0224			
TRBV8-2	3.412	1.18E-25	<0.0001			
PPP2R5C	3.377	2.13E-04	0.0111			
PLXDC1	3.344	7.88E-38	0.0000	●	●	
TMEM91	3.320	6.58E-05	0.0043			
COBLL1	3.279	6.35E-04	0.0267		●	
CD200R1	3.256	8.72E-04	0.0343	●		
ATN1	3.171	1.80E-04	0.0097	●		
SIGIRR	3.166	5.92E-04	0.0253		●	
TNNT3	3.164	7.21E-04	0.0296			●
LRP1	3.159	8.14E-04	0.0326			
FGD1	3.044	1.13E-03	0.0421			●
Lower in OxPhosi-treated AML cells than in vehicle-treated cells						
IGLL5	−7.753	1.25E-06	0.0001			
IGLV1-44	−6.834	3.23E-05	0.0023			
RIBC2	−6.631	1.43E-05	0.0012			
RAB39A	−6.591	3.79E-06	0.0004			
GLRA3	−6.351	9.65E-05	0.0059			
PAX5	−6.235	1.83E-04	0.0099			
KLRC2	−6.222	1.19E-04	0.0070			
SYK	−6.093	3.04E-05	0.0022			
NPM1P18	−6.050	4.71E-05	0.0032			
HCK	−5.913	7.38E-04	0.0300			
BCAR3	−5.889	5.85E-04	0.0251			
CD82	−5.753	2.20E-04	0.0115			
TCL1A	−5.599	2.36E-04	0.0121			
TNS3	−5.582	3.13E-05	0.0023			
TLE1	−5.480	6.57E-04	0.0274			
TCEB2P2	−5.405	3.34E-05	0.0024			
H2BFS	−5.352	2.27E-05	0.0017			
ABCB4	−5.242	2.19E-04	0.0114			
AP3B1	−5.154	1.47E-05	0.0012			
AK097298	−5.074	1.17E-04	0.0069			
NAPSB	−5.026	6.93E-05	0.0044			
TUBB3	−4.855	1.81E-04	0.0098			

Table 4. (continued)

Gene name	Log_2 fold change	*P*	FDR	Adhesion	Migration	Actin cytoskeleton dynamics
SPIN4	−4.851	1.91E-04	0.0102			
HIST3H2A	−4.794	5.91E-04	0.0253			
TP63	−4.766	4.31E-04	0.0197			
LILRB4	−4.748	3.38E-04	0.0163			
PLA2G2D	−4.713	1.99E-04	0.0106			
SPTY2D1	−4.711	2.16E-04	0.0113			
RNF2	−4.689	6.34E-05	0.0041			
PLXNA4	−4.667	2.22E-04	0.0115			
LINC00152	−4.622	1.10E-03	0.0411			
RNU5A-8P	−4.584	9.07E-05	0.0056			
GFPT1	−4.583	9.14E-05	0.0056			
THAP2	−4.580	1.03E-04	0.0062			
FADS2	−4.578	2.10E-04	0.0110			
FCRLA	−4.576	6.86E-04	0.0284			
AIM2	−4.528	1.05E-03	0.0395			
CDK14	−4.519	4.90E-04	0.0217			
CCND1	−4.514	5.39E-04	0.0235			
CHL1	−4.442	6.22E-04	0.0263			
HIST3H2BB	−4.412	9.05E-05	0.0056			
GCN1L1	−4.344	8.47E-04	0.0335			
RERE	−4.332	3.72E-04	0.0176			
TIAM1	−4.329	3.54E-04	0.0169			
CEND1	−4.264	1.17E-03	0.0433			
SYVN1	−4.253	1.05E-03	0.0396			
KYNU	−4.235	1.76E-04	0.0095			
RPL17P20	−4.223	1.59E-04	0.0088			
uc001tcg.1	−4.217	3.88E-04	0.0182			
ARHGEF7	−4.196	1.27E-03	0.0461			
IL10	−4.188	6.53E-04	0.0273			
SMS	−4.183	8.23E-04	0.0328			
PI16	−4.137	2.82E-19	0.0000			
TP53I11	−4.102	7.22E-04	0.0296			
CD24	−4.075	8.40E-05	0.0052			
RPL35P2	−4.029	1.56E-05	0.0013			
MPEG1	−3.923	3.46E-04	0.0165			
ZNF804A	−3.919	1.07E-04	0.0064			
IL28RA	−3.882	8.71E-04	0.0343			
FCHSD2	−3.879	5.96E-04	0.0254			
SPIB	−3.875	3.25E-04	0.0158			
RPL34P23	−3.873	2.81E-05	0.0021			
ALOX5	−3.695	3.73E-04	0.0176			
VPREB3	−3.683	1.36E-03	0.0488			
NXT2	−3.621	1.35E-04	0.0077			
PPIAP29	−3.607	1.63E-04	0.0089			
DPP3	−3.594	2.08E-05	0.0016			
SNX9	−3.505	1.49E-04	0.0083			
ENPP2	−3.496	3.45E-04	0.0165			
FA2H	−3.486	6.14E-04	0.0260			

Table 4. (continued)

Gene name	Log_2 fold change	*P*	FDR	Adhesion	Migration	Actin cytoskeleton dynamics
PLD4	−3.484	3.35E-04	0.0162			
TPD52	−3.470	3.98E-04	0.0185			
IGKV1D-33	−3.435	8.34E-04	0.0331			
SFN	−3.420	3.09E-09	<0.0001			
MS4A1	−3.368	1.60E-04	0.0089			
PHACTR1	−3.357	3.98E-05	0.0028			
PHLDB2	−3.263	3.59E-04	0.0170			
PLAC8	−3.258	2.05E-04	0.0108			
DARS	−3.224	2.10E-05	0.0016			
IL18R1	−3.198	4.21E-12	<0.0001			
TNFRSF13B	−3.179	8.15E-04	0.0326			
SLC20A2	−3.164	7.41E-04	0.0302			
HIST2H3A, HIST2H3C, HIST2H3D	−3.153	1.08E-04	0.0064			
TPPP3	−3.148	1.07E-16	<0.0001			
PELO	−3.111	2.95E-09	<0.0001			
RPL14P1	−3.102	1.72E-05	0.0014			
RASSF6	−3.100	9.19E-04	0.0358			
HMGA1P3	−3.071	3.51E-04	0.0167			
MSL1	−3.067	1.13E-03	0.0421			
PDE4D	−3.064	8.73E-04	0.0343			
HBEGF	−3.047	4.75E-04	0.0213			
RIC8B	−3.027	7.72E-04	0.0311			
PDE4B	−3.027	1.21E-06	0.0001			

Table 5. Significantly altered promoter expression in OxPhosi-sensitive and OxPhosi-resistant AML cells after OxPhosi treatment in vivo

	OxPhosi-sensitive			OxPhosi-resistant			
Patient No.	**27**	**28**	**29**	**30**	**31**	**32**	**33**
CCR8	NC	NC	NC	Up	Up	Up	Up
BAI2	NC	NC	NC	Up	Up	Up	Up
LAG3	NC	NC	NC	Up	Up	NC	Up
ATN1	Down	Down	NC	Up	Up	Up	NC
PLXDC1	NC	NC	NC	Up	Up	Up	Up

Down, downregulated by OxPhosi treatment; NC, no significant change with OxPhosi treatment; Up, upregulated by OxPhosi treatment.

OxPhosi-treated AML cells in vivo. ASS1 is a key enzyme in the biosynthesis of arginine,[52] and LRP1 plays a major role in lipid metabolism and is responsible for hemin-induced autophagy in leukemia cells.[53,74] Additional experiments are required to address the role of these enzymes in the responses of AML cells to the metabolic and energetic consequences of OxPhos inhibition.

In conclusion, this study demonstrates that exogenous mitochondrial transfer and endogenous mitochondrial fission in AML cells serve as compensatory adaptations to OxPhos inhibition in the BM microenvironment. The BM microenvironment thereby facilitates secondary resistance to OxPhos inhibition by modulating mitochondrial functions; interference with these processes is required to boost the antitumor potency of OxPhos inhibition.

Acknowledgments

The authors are grateful to Kaoru Mogushi, Masaki Hosoya, Takashi Ueno, and Masaaki Komatsu for useful discussions and to Akemi Kawasaki for technical assistance. The authors thank the Laboratories of Molecular and Biochemical Research and Cell Biology Research and the Division of Proteomics and BioMolecular Science, Juntendo University Graduate School of Medicine for use of their facilities, and Amy Ninetto, Research Medical Library at MD Anderson Cancer Center for manuscript review.

This work was supported in part by grants from the Japan Society for the Promotion of Science Grants-in Aid for Scientific Research (18K07424) (Y.T.), from International Joint Research Programs (19KK0221) (Y.T.), from Platform Project for Supporting

Drug Discovery and Life Science Research (Basis for Supporting Innovative Drug Discovery and Life Science Research) from the Japan Agency for Medical Research and Development (JP17am0101102) (Y.T.), National Cancer Institute, National Institutes of Health Specialized Programs of Research Excellence in Leukemia Project 5 (P50 CA100632-16) (M.K.), from the Cancer Prevention & Research Institute of Texas (RP180309 and RP160693) (M.K.), and the MD Anderson Cancer Center Sister Institution Network Fund (M.K.).

Authorship

Contribution: M.K. and Y.T. designed the study; H.Y., Q.Z., K. Saito, and K.Y. performed experiments and analyzed data; T.A. designed experiments and wrote the paper; V.R., N.B., T.C., H.M., R.J., V.K., K.M., and K. Suzuki performed experiments; T.M. and Y.-M.K. discussed experiments; J.I., S.K., and K.I. were involved in statistical analysis; C.P.V., M.A., and J.R.M. discussed experiments and helped interpret data; and all authors critically reviewed and revised the manuscript for content and approved the manuscript for publication.

Conflicts-of-interest disclosure: The authors declare no competing financial interests.

ORCID profiles: K.Y., 0000-0002-0162-1162; T.A., 0000-0003-0376-0227; V.R., 0000-0003-4363-7258; N.B., 0000-0003-0618-4798; T.M., 0000-0002-4294-8030; Y.-M.K., 0000-0003-3793-6438; M.A., 0000-0002-1144-1958; Y.T., 0000-0002-3734-0346; M.K., 0000-0002-9347-2212.

Correspondence: Marina Konopleva, Department of Leukemia, The University of Texas MD Anderson Cancer Center, 1400 Holcombe Blvd, FC3.3048, Houston, TX 77030; e-mail: mkonople@mdanderson.org; and Yoko Tabe, Department of Clinical Laboratory Medicine, Juntendo University Graduate School of Medicine, 2-1-1 Hongo, Bunkyo City, Tokyo 113-8421, Japan; e-mail: tabe@juntendo.ac.jp.

References

1. Zhao Y, Butler EB, Tan M. Targeting cellular metabolism to improve cancer therapeutics. *Cell Death Dis.* 2013;4(3):e532.
2. Frolova O, Samudio I, Benito JM, et al. Regulation of HIF-1α signaling and chemoresistance in acute lymphocytic leukemia under hypoxic conditions of the bone marrow microenvironment. *Cancer Biol Ther.* 2012;13(10):858-870.
3. Benito J, Shi Y, Szymanska B, et al. Pronounced hypoxia in models of murine and human leukemia: high efficacy of hypoxia-activated prodrug PR-104. *PLoS One.* 2011;6(8):e23108.
4. Skrtić M, Sriskanthadevan S, Jhas B, et al. Inhibition of mitochondrial translation as a therapeutic strategy for human acute myeloid leukemia. *Cancer Cell.* 2011;20(5):674-688.
5. Lagadinou ED, Sach A, Callahan K, et al. BCL-2 inhibition targets oxidative phosphorylation and selectively eradicates quiescent human leukemia stem cells. *Cell Stem Cell.* 2013;12(3):329-341.
6. Gut P, Verdin E. The nexus of chromatin regulation and intermediary metabolism. *Nature.* 2013;502(7472):489-498.
7. Viale A, Pettazzoni P, Lyssiotis CA, et al. Oncogene ablation-resistant pancreatic cancer cells depend on mitochondrial function. *Nature.* 2014;514(7524):628-632.
8. Molina JR, Sun Y, Protopopova M, et al. An inhibitor of oxidative phosphorylation exploits cancer vulnerability. *Nat Med.* 2018;24(7):1036-1046.
9. Marlein CR, Zaitseva L, Piddock RE, et al. NADPH oxidase-2 derived superoxide drives mitochondrial transfer from bone marrow stromal cells to leukemic blasts. *Blood.* 2017;130(14):1649-1660.
10. Burt R, Dey A, Aref S, et al. Activated stromal cells transfer mitochondria to rescue acute lymphoblastic leukemia cells from oxidative stress. *Blood.* 2019;134(17):1415-1429.
11. Moschoi R, Imbert V, Nebout M, et al. Protective mitochondrial transfer from bone marrow stromal cells to acute myeloid leukemic cells during chemotherapy. *Blood.* 2016;128(2):253-264.
12. Murray LMA, Krasnodembskaya AD. Concise review: Intercellular communication via organelle transfer in the biology and therapeutic applications of stem cells. *Stem Cells.* 2019;37(1):14-25.
13. Johnson EA, Marks RS, Mandrekar SJ, et al. Phase III randomized, double-blind study of maintenance CAI or placebo in patients with advanced non-small cell lung cancer (NSCLC) after completion of initial therapy (NCCTG 97-24-51). *Lung Cancer.* 2008;60(2):200-207.
14. Ellinghaus P, Heisler I, Unterschemmann K, et al. BAY 87-2243, a highly potent and selective inhibitor of hypoxia-induced gene activation has antitumor activities by inhibition of mitochondrial complex I. *Cancer Med.* 2013;2(5):611-624.
15. Milella M, Kornblau SM, Estrov Z, et al. Therapeutic targeting of the MEK/MAPK signal transduction module in acute myeloid leukemia. *J Clin Invest.* 2001;108(6):851-859.
16. Takahashi H, Lassmann T, Murata M, Carninci P. 5' end-centered expression profiling using cap-analysis gene expression and next-generation sequencing. *Nat Protoc.* 2012;7(3):542-561.
17. Wang L, Feng Z, Wang X, Wang X, Zhang X. DEGseq: an R package for identifying differentially expressed genes from RNA-seq data. *Bioinformatics.* 2010;26(1):136-138.
18. Ohmiya H, Vitezic M, Frith MC, et al; FANTOM Consortium. RECLU: a pipeline to discover reproducible transcriptional start sites and their alternative regulation using capped analysis of gene expression (CAGE). *BMC Genomics.* 2014;15(1):269.
19. Subramanian A, Tamayo P, Mootha VK, et al. Gene set enrichment analysis: a knowledge-based approach for interpreting genome-wide expression profiles. *Proc Natl Acad Sci U S A.* 2005;102(43):15545-15550.

20. Gang EJ, Kim HN, Hsieh YT, et al. Integrin α6 mediates the drug resistance of acute lymphoblastic B-cell leukemia. *Blood.* 2020;136(2):210-223.
21. Vangapandu HV, Havranek O, Ayres ML, et al. B-cell receptor signaling regulates metabolism in chronic lymphocytic leukemia. *Mol Cancer Res.* 2017; 15(12):1692-1703.
22. König J, Ott C, Hugo M, et al. Mitochondrial contribution to lipofuscin formation. *Redox Biol.* 2017;11:673-681.
23. Kawaji H, Lizio M, Itoh M, et al; FANTOM Consortium. Comparison of CAGE and RNA-seq transcriptome profiling using clonally amplified and single-molecule next-generation sequencing. *Genome Res.* 2014;24(4):708-717.
24. Warton K, Foster NC, Gold WA, Stanley KK. A novel gene family induced by acute inflammation in endothelial cells. *Gene.* 2004;342(1):85-95.
25. De Falco V, Castellone MD, De Vita G, et al. RET/papillary thyroid carcinoma oncogenic signaling through the Rap1 small GTPase. *Cancer Res.* 2007; 67(1):381-390.
26. Samsonraj RM, Paradise CR, Dudakovic A, et al. Validation of osteogenic properties of cytochalasin D by high-resolution RNA-sequencing in mesenchymal stem cells derived from bone marrow and adipose tissues. *Stem Cells Dev.* 2018;27(16):1136-1145.
27. Colicelli J. Human RAS superfamily proteins and related GTPases. *Sci STKE.* 2004;2004(250):RE13.
28. Wang J, Liu X, Qiu Y, et al. Cell adhesion-mediated mitochondria transfer contributes to mesenchymal stem cell-induced chemoresistance on T cell acute lymphoblastic leukemia cells. *J Hematol Oncol.* 2018;11(1):11.
29. Bradstock KF, Gottlieb DJ. Interaction of acute leukemia cells with the bone marrow microenvironment: implications for control of minimal residual disease. *Leuk Lymphoma.* 1995;18(1-2):1-16.
30. Winter SS, Sweatman JJ, Lawrence MB, Rhoades TH, Hart AL, Larson RS. Enhanced T-lineage acute lymphoblastic leukaemia cell survival on bone marrow stroma requires involvement of LFA-1 and ICAM-1. *Br J Haematol.* 2001;115(4):862-871.
31. Damiano JS, Cress AE, Hazlehurst LA, Shtil AA, Dalton WS. Cell adhesion mediated drug resistance (CAM-DR): role of integrins and resistance to apoptosis in human myeloma cell lines. *Blood.* 1999;93(5):1658-1667.
32. Hsieh YT, Gang EJ, Geng H, et al. Integrin alpha4 blockade sensitizes drug resistant pre-B acute lymphoblastic leukemia to chemotherapy. *Blood.* 2013;121(10):1814-1818.
33. Kim I, Rodriguez-Enriquez S, Lemasters JJ. Selective degradation of mitochondria by mitophagy. *Arch Biochem Biophys.* 2007;462(2):245-253.
34. Wallace DC. Mitochondria and cancer: Warburg addressed. *Cold Spring Harb Symp Quant Biol.* 2005;70(0):363-374.
35. Mizushima N, Komatsu M. Autophagy: renovation of cells and tissues. *Cell.* 2011;147(4):728-741.
36. Ding Y, Yang J, Chen P, et al. Knockout of SORBS2 protein disrupts the structural integrity of intercalated disc and manifests features of arrhythmogenic cardiomyopathy. *J Am Heart Assoc.* 2020;9(17):e017055.
37. Oshio T, Kawashima R, Kawamura YI, et al. Chemokine receptor CCR8 is required for lipopolysaccharide-triggered cytokine production in mouse peritoneal macrophages. *PLoS One.* 2014;9(4):e94445.
38. Purcell RH, Toro C, Gahl WA, Hall RA. A disease-associated mutation in the adhesion GPCR BAI2 (ADGRB2) increases receptor signaling activity. *Hum Mutat.* 2017;38(12):1751-1760.
39. Huard B, Mastrangeli R, Prigent P, et al. Characterization of the major histocompatibility complex class II binding site on LAG-3 protein. *Proc Natl Acad Sci U S A.* 1997;94(11):5744-5749.
40. Yamaji Y, Yoshida S, Ishikawa K, et al. TEM7 (PLXDC1) in neovascular endothelial cells of fibrovascular membranes from patients with proliferative diabetic retinopathy. *Invest Ophthalmol Vis Sci.* 2008;49(7):3151-3157.
41. Ko YC, Chien HF, Jiang-Shieh YF, et al. Endothelial CD200 is heterogeneously distributed, regulated and involved in immune cell-endothelium interactions. *J Anat.* 2009;214(1):183-195.
42. Loers G, Makhina T, Bork U, Dörner A, Schachner M, Kleene R. The interaction between cell adhesion molecule L1, matrix metalloproteinase 14, and adenine nucleotide translocator at the plasma membrane regulates L1-mediated neurite outgrowth of murine cerebellar neurons. *J Neurosci.* 2012;32(11): 3917-3930.
43. Liu X, Xu X, Deng W, et al. CCL18 enhances migration, invasion and EMT by binding CCR8 in bladder cancer cells. *Mol Med Rep.* 2019;19(3):1678-1686.
44. Zhang ZZ, Hua R, Zhang JF, et al. TEM7 (PLXDC1), a key prognostic predictor for resectable gastric cancer, promotes cancer cell migration and invasion. *Am J Cancer Res.* 2015;5(2):772-781.
45. Takayama KI, Suzuki T, Fujimura T, Takahashi S, Inoue S. COBLL1 modulates cell morphology and facilitates androgen receptor genomic binding in advanced prostate cancer. *Proc Natl Acad Sci U S A.* 2018;115(19):4975-4980.
46. Guo J, Zhan X, Xu G, Mao C, Wei R. Transcriptomic analysis reveals that IL-1R8/Sigirr is a novel macrophage migration regulator and suppresses macrophage proliferation through p38 MAPK signaling pathway. *Biomed Pharmacother.* 2020;124:109846.
47. Delgado M, Tesfaigzi Y. BH3-only proteins, Bmf and Bim, in autophagy. *Cell Cycle.* 2013;12(22):3453-3454.
48. Mladenova K, Petrova S, Moskova-Doumanova V, et al. Transepithelial resistance in human bestrophin-1 stably transfected Madin-Darby canine kidney cells. *Biotechnol Biotechnol Equip.* 2015;29(1):101-104.
49. Wei B, Jin JP. TNNT1, TNNT2, and TNNT3: isoform genes, regulation, and structure-function relationships. *Gene.* 2016;582(1):1-13.
50. Hou P, Estrada L, Kinley AW, Parsons JT, Vojtek AB, Gorski JL. Fgd1, the Cdc42 GEF responsible for faciogenital dysplasia, directly interacts with cortactin and mAbp1 to modulate cell shape. *Hum Mol Genet.* 2003;12(16):1981-1993.

51. Miraki-Moud F, Ghazaly E, Ariza-McNaughton L, et al. Arginine deprivation using pegylated arginine deiminase has activity against primary acute myeloid leukemia cells in vivo. *Blood.* 2015;125(26):4060-4068.
52. Syed N, Langer J, Janczar K, et al. Epigenetic status of argininosuccinate synthetase and argininosuccinate lyase modulates autophagy and cell death in glioblastoma. *Cell Death Dis.* 2013;4(1):e458.
53. Xing P, Liao Z, Ren Z, et al. Roles of low-density lipoprotein receptor-related protein 1 in tumors. *Chin J Cancer.* 2016;35(1):6.
54. Gardeitchik T, Mohamed M, Ruzzenente B, et al. Bi-allelic mutations in the mitochondrial ribosomal protein MRPS2 cause sensorineural hearing loss, hypoglycemia, and multiple OXPHOS complex deficiencies. *Am J Hum Genet.* 2018;102(4):685-695.
55. Razmkhah F, Ghasemi S, Soleimani M, Amini Kafi-Abad S. LY86, LRG1 and PDE9A genes overexpression in umbilical cord blood hematopoietic stem progenitor cells by acute myeloid leukemia (M3) microvesicles. *Exp Hematol Oncol.* 2019;8(1):23.
56. Lou E, Fujisawa S, Morozov A, et al. Tunneling nanotubes provide a unique conduit for intercellular transfer of cellular contents in human malignant pleural mesothelioma. *PLoS One.* 2012;7(3):e33093.
57. Wang X, Gerdes HH. Transfer of mitochondria via tunneling nanotubes rescues apoptotic PC12 cells. *Cell Death Differ.* 2015;22(7):1181-1191.
58. Islam MN, Das SR, Emin MT, et al. Mitochondrial transfer from bone-marrow-derived stromal cells to pulmonary alveoli protects against acute lung injury. *Nat Med.* 2012;18(5):759-765.
59. Tan AS, Baty JW, Dong LF, et al. Mitochondrial genome acquisition restores respiratory function and tumorigenic potential of cancer cells without mitochondrial DNA. *Cell Metab.* 2015;21(1):81-94.
60. Farge T, Saland E, de Toni F, et al. Chemotherapy-resistant human acute myeloid leukemia cells are not enriched for leukemic stem cells but require oxidative metabolism. *Cancer Discov.* 2017;7(7):716-735.
61. Zhuo M, Gorgun MF, Englander EW. Neurotoxicity of cytarabine (Ara-C) in dorsal root ganglion neurons originates from impediment of mtDNA synthesis and compromise of mitochondrial function. *Free Radic Biol Med.* 2018;121:9-19.
62. Abounit S, Delage E, Zurzolo C. Identification and characterization of tunneling nanotubes for intercellular trafficking. *Curr Protoc Cell Biol.* 2015;67:12.10.1-12.10.21.
63. Biran A, Perelmutter M, Gal H, et al. Senescent cells communicate via intercellular protein transfer. *Genes Dev.* 2015;29(8):791-802.
64. Frei DM, Hodneland E, Rios-Mondragon I, et al. Novel microscopy-based screening method reveals regulators of contact-dependent intercellular transfer. *Sci Rep.* 2015;5(1):12879.
65. Ridley AJ. Rho GTPase signalling in cell migration. *Curr Opin Cell Biol.* 2015;36:103-112.
66. Mistry JJ, Marlein CR, Moore JA, et al. ROS-mediated PI3K activation drives mitochondrial transfer from stromal cells to hematopoietic stem cells in response to infection. *Proc Natl Acad Sci U S A.* 2019;116(49):24610-24619.
67. Iqbal S, Hood DA. Oxidative stress-induced mitochondrial fragmentation and movement in skeletal muscle myoblasts. *Am J Physiol Cell Physiol.* 2014;306(12):C1176-C1183.
68. Kim DY, Jung SY, Kim YJ, et al. Hypoxia-dependent mitochondrial fission regulates endothelial progenitor cell migration, invasion, and tube formation. *Korean J Physiol Pharmacol.* 2018;22(2):203-213.
69. Toyama EQ, Herzig S, Courchet J, et al. Metabolism. AMP-activated protein kinase mediates mitochondrial fission in response to energy stress. *Science.* 2016;351(6270):275-281.
70. Cai J, Wang J, Huang Y, et al. ERK/Drp1-dependent mitochondrial fission is involved in the MSC-induced drug resistance of T-cell acute lymphoblastic leukemia cells. *Cell Death Dis.* 2016;7(11):e2459.
71. Pei S, Minhajuddin M, Adane B, et al. AMPK/FIS1-mediated mitophagy is required for self-renewal of human AML stem cells. *Cell Stem Cell.* 2018;23(1):86-100.e6.
72. Jiang D, Chen FX, Zhou H, et al. Bioenergetic crosstalk between mesenchymal stem cells and various ocular cells through the intercellular trafficking of mitochondria. *Theranostics.* 2020;10(16):7260-7272.
73. Sriskanthadevan S, Jeyaraju DV, Chung TE, et al. AML cells have low spare reserve capacity in their respiratory chain that renders them susceptible to oxidative metabolic stress. *Blood.* 2015;125(13):2120-2130.
74. Grosso RA, Caldarone PVS, Sánchez MC, Chiabrando GA, Colombo MI, Fader CM. Hemin induces autophagy in a leukemic erythroblast cell line through the LRP1 receptor. *Biosci Rep.* 2019;39(1):BSR20181156.